

DTP-97/29
June 1997
hep-th/9706140

Excited states in some simple perturbed conformal field theories

Patrick Dorey and Roberto Tateo

*Department of Mathematical Sciences,
University of Durham, Durham DH1 3LE, England**

Abstract

The method of analytic continuation is used to find exact integral equations for a selection of finite-volume energy levels for the non-unitary minimal models $\mathcal{M}_{2,2N+3}$ perturbed by their φ_{13} operators. The $N=2$ case is studied in particular detail. Along the way, we find a number of general results which should be relevant to the study of excited states in other models.

PACS numbers: 05.50+q, 11.25.Hf, 64.60.Ak, 75.10.Hk

*e-mail: P.E.Dorey@durham.ac.uk, Roberto.Tateo@durham.ac.uk

1 Introduction

The finite-volume spectrum of a quantum field theory encodes a great deal of information, of interest even if the ultimate objective is to understand the behaviour of the theory in a world of infinite extent [1, 2]. In the unusually tractable examples provided by integrable theories in 1+1 dimensions, it has been known for some time that an effective way to obtain the lowest level of this spectrum (the ground-state energy) is provided by the integral equations of the thermodynamic Bethe ansatz, or TBA [3]. More recently, modifications to these equations have been found which extend the treatment to other (‘excited’) energy levels, for the rather simple but nonetheless nontrivial case of the scaling Lee-Yang model, or SLYM [4, 5]. (An alternative approach, based on the Destri – de Vega equation, was initiated in refs. [6], but its relation with the TBA remains to be understood.) In this paper we explore how the methods of [5] can be generalised to a series of models, namely the perturbations of the minimal models $\mathcal{M}_{2,2N+3}$ by their φ_{13} operators. Apart from $N=1$, which is just the scaling Lee-Yang model, these theories all have more than one mass in their spectrum, and their excited-state TBA equations exhibit a number of new phenomena. The bulk of the paper concerns the $N=2$ case, for which we have some detailed numerical results. For higher values of N , our results are less complete, though we can be confident that we have captured the exact behaviour of the one-particle levels in the infrared region.

The paper begins with a brief review of the relevant perturbed conformal field theories, and a discussion of some general properties of TBA equations that will be important later. Ref. [5] can be consulted for some further background on the idea of analytic continuation as applied to TBA systems. In section 3 the method is used to give a reasonably complete analysis of the first few levels for $N=2$, whilst section 4 describes some features which emerge when the same techniques are applied to the other theories. None of these models is of overwhelming physical importance, and our main aim has been to use them as a testing-ground for the whole analytic continuation approach to generalised TBA equations. With this in mind, the concluding section 5 includes a summary of those features which have emerged during our investigations that should have wider applicability. There are two appendices: the first recalls some field-theoretic predictions for infrared asymptotics, and the second compares the numerical solutions of our equations with results obtained from the truncated conformal space approach.

2 The T_N -related perturbed conformal field theories

The minimal models $\mathcal{M}_{2,2N+3}$ have $N+1$ primary fields $\varphi_{1,s}$, occupying a single row of the Kac table. The central charge is $c = -2N(6N+5)/(2N+3)$, and the scaling dimensions of the primary fields are

$$d_{1,s} = -\frac{(s-1)(2N+2-s)}{2N+3} \quad s = 1 \dots N+1 .$$

Perturbing by φ_{13} results in a factorised scattering theory sometimes denoted by T_N , or else $A_{2N}^{(2)}$ [7, 8]. This has N self-conjugate particles with masses M_a :

$$M_a = \frac{\sin(\pi a/h)}{\sin(\pi/h)} M_1 \quad a = 1 \dots N ,$$

where $h = 2N+1$, and two-particle S-matrix elements $S_{ab}(\theta)$:

$$S_{ab} = \prod_{\substack{|a-b|+1 \\ \text{step } 2}}^{a+b-1} \{l\} \{h-l\} \quad (a, b = 1 \dots N) ; \quad (2.1)$$

$$\{x\} = (x-1)(x+1) \quad ; \quad (x)(\theta) = \frac{\sinh(\frac{\theta}{2} + \frac{i\pi x}{2h})}{\sinh(\frac{\theta}{2} - \frac{i\pi x}{2h})} .$$

The exact relation between the φ_{13} coupling λ and the mass M_1 of the lightest particle was found by Al.B.Zamolodchikov [9]. Setting $g(x) = \sqrt{\Gamma(x)/\Gamma(1-x)}$, it is

$$M_1(\lambda) = \frac{4 \sin \frac{\pi}{h}}{\sqrt{\pi}} \frac{\Gamma(\frac{1}{h})}{\Gamma(\frac{1}{2} + \frac{1}{h})} \left[\pi \frac{(h-2)(h-4)}{(h+2)^2} g\left(\frac{h-4}{h+2}\right) g\left(\frac{h}{h+2}\right) \right]^{\frac{h+2}{4h}} (-\lambda)^{\frac{h+2}{4h}} , \quad (2.2)$$

In the normalisations implicit in [9], a sensible scattering theory with real masses for the particles is obtained when the coupling λ is real and *negative*. The only exception is $N=1$, where the imaginary values of some conformal structure constants mean that a real perturbative expansion is obtained if λ is purely imaginary, and $\text{Im } \lambda$ must be positive for real masses in the infrared [3, 10].

Since the S-matrix (2.1) is diagonal, the TBA equations for the ground state energy on a circle of circumference R are [3, 11]:

$$\varepsilon_a(\theta) = m_a r \cosh \theta - \sum_{b=1}^N \phi_{ab}^* L_b(\theta) , \quad (2.3)$$

with

$$r = M_1 R, \quad m_a = \frac{M_a}{M_1}, \quad \phi_{ab}(\theta) = -i \frac{\partial}{\partial \theta} \log S_{ab}(\theta), \quad L_a(\theta) = \log \left(1 + e^{-\varepsilon_a(\theta)} \right),$$

and $f * g(\theta)$ denoting the convolution $\frac{1}{2\pi} \int_{-\infty}^{\infty} d\theta' f(\theta - \theta') g(\theta')$. Solving these equations yields N pseudoenergies $\varepsilon_a(\theta)$; the ground state energy is then

$$E_0(\lambda, R) = E_{\text{bulk}}(\lambda, R) - \frac{\pi}{6R} c(r);$$

$$E_{\text{bulk}}(\lambda, R) = -\frac{M_1(\lambda)^2}{8 \sin(2\pi/h)} R, \quad c(r) = \frac{3}{\pi^2} \sum_{a=1}^N \int_{-\infty}^{\infty} d\theta r \cosh \theta L_a(\theta). \quad (2.4)$$

It will sometimes be convenient to work with the scaling functions $F_i(r)$, related to the energy levels E_i by $E_i(\lambda, R) = \frac{2\pi}{R} F_i(M_1 R)$.

The functions $Y_a(\theta) = \exp(\varepsilon_a(\theta))$ provide an r -dependent set of solutions to a set of functional relations called a Y-system [12, 13]

$$Y_a\left(\theta - \frac{i\pi}{h}\right) Y_a\left(\theta + \frac{i\pi}{h}\right) = \prod_{b=1}^N (1 + Y_b(\theta))^{l_{ab}^{[T_N]}}, \quad (2.5)$$

where $l_{ab}^{[T_N]} = \delta_{a,b-1} + \delta_{a,b+1} + \delta_{a,N} \delta_{b,N}$ is the incidence matrix of the T_N graph. A (none-too-obvious) consequence of these equations is that the functions $Y_a(\theta)$ are $i\pi(h+2)/h$ -periodic:

$$Y_a\left(\theta + \frac{i\pi(h+2)}{h}\right) = Y_a(\theta). \quad (2.6)$$

Subtracting the right-hand side of (2.5) from the left-hand side yields an analytic function of r and θ which is identically zero. This function therefore remains zero during any process of analytic continuation, and so the Y-system and all of its consequences hold equally for all the continuations of the basic TBA to be encountered below. With this in mind, it is worth pausing to record a couple of other general properties before proceeding to specific examples.

The first concerns the behaviour of the Y_a as functions of r and θ combined. If we define a new pair of variables as follows:

$$a_+ = \left(r e^\theta \right)^{2h/(h+2)} \quad ; \quad a_- = \left(r e^{-\theta} \right)^{2h/(h+2)} \quad (2.7)$$

then we claim that each $Y_a(a_+, a_-)$ can be expanded as a power series about $a_+ = a_- = 0$, with a finite domain $\mathcal{D} \subset \mathbb{C} \times \mathbb{C}$ of convergence. This is a

conjecture, but note that it corresponds to an expansion about the central region in the ‘kink limit’ of the TBA, where we would not expect to find any singularities, all pseudoenergies tending to constants there.

The second general property follows from the first. Consider simultaneous changes of r and θ which leave a_+ and a_- invariant. These take the form $r \rightarrow e^{i\alpha}r$; $\theta \rightarrow \theta + i\beta$ with $\alpha = (p+q)\pi(h+2)/2h$, $\beta = (p-q)\pi(h+2)/2h$, and (p, q) a pair of integers. The $(-1, 0)$ case of this transformation shows that

$$Y_a(e^{-i\pi(h+2)/2h}r, \theta - i\pi\frac{h+2}{2h}) = Y_a(r, \theta) \quad ((a_+, a_-) \in \mathcal{D}). \quad (2.8)$$

This result is only guaranteed while $|r|$ and $|\theta|$ are small enough that (a_+, a_-) lies in \mathcal{D} . However as functions of θ alone, the Y_a are expected to be entire (in the conformal case this can be proved in some situations [4]). If $|r|$ is sufficiently small, then (a_+, a_-) will lie in \mathcal{D} for, say, real θ in the unit interval; the identity (2.8) holds for these values of θ , and can then be analytically continued to all θ while r remains fixed. Using the real analyticity of the Y ’s we can then deduce that for these sufficiently small values of $|r|$ the functions $Y_a(r, \theta)$ have the symmetry

$$Y_a(r, \theta) = Y_a^*(\tilde{r}, \tilde{\theta}) \quad (2.9)$$

where

$$\tilde{r} = e^{i\pi(h+2)/2h}r^* \quad , \quad \tilde{\theta} = i\pi\frac{h+2}{2h} + \theta^* \quad (2.10)$$

and the asterisks denote complex conjugation. For larger values of $|r|$, the point (a_+, a_-) will be outside \mathcal{D} for all θ , and the argument breaks down. Indeed, the functions $Y_a(r, \theta)$ acquire a multi-valued structure reflecting the multivalued nature of the energy levels themselves. However, since all of these functions can be found by analytic continuation from the small- $|r|$ region, a memory of the earlier relation remains in an involution on the set of all Y ’s: given a function $Y_a(r, \theta)$, the exponential of the solution to some (perhaps generalised) TBA equation, another function $\tilde{Y}_a(r, \theta)$ can be defined by

$$\tilde{Y}_a(\tilde{r}, \theta) = Y_a^*(r, \tilde{\theta}) . \quad (2.11)$$

The logarithm of this function, $\tilde{\varepsilon}_a(\theta) = \log \tilde{Y}_a(\tilde{r}, \theta)$, will again solve a (possibly different) TBA equation, with the radius r replaced by the reflected radius \tilde{r} . The observation turns out to be rather useful, allowing solutions of the generalised TBA equations to be obtained in some situations where a direct numerical attack fails. So as not to have to rely for it on the power-series expansion, we also checked its validity, for $N=2, 3$ and 4 , in various

situations where the equations related to both Y_a and \tilde{Y}_a could be solved numerically.

3 Excited states for $\mathcal{M}_{2,7} + \lambda\varphi_{13}$

In this section we restrict our attention to the case $N=2, h=5$. The approach proposed in [5] requires the continuation of r along some path in the complex plane, in the hope of inducing a monodromy in $c(r)$ which will convert the ground state into an excited state. To decide which paths to take, we used the truncated conformal space approach (TCSA) [10], and in particular the program of ref. [14], to map the first few sheets of the Riemann surface associated with the ground state scaling function $F_0(r)$. The results are shown schematically in figure 1.

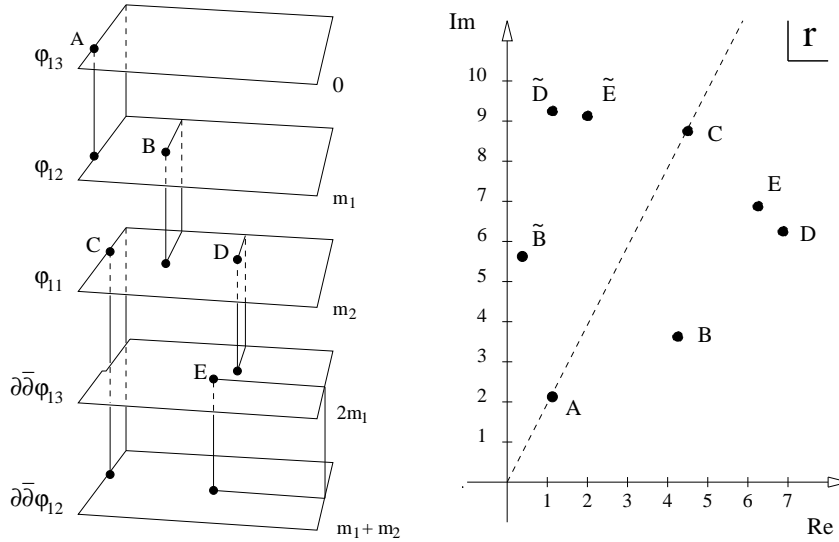


Figure 1: The first five sheets of the Riemann surface of the scaling function $F(r)$, showing on the left the connectivity of the various sheets, and on the right the positions of the square-root branch points over the complex r -plane.

Figures 2 and 3 may also help to visualise how the sheets fit together. Figure 2 plots various $F(r)$ for real values of r between 0 and 12, labelling the lines both by their ultraviolet limits near $r=0$, and by their asymptotic mass gaps at large r . Figure 3 shows the real parts of these same $F(r)$ along

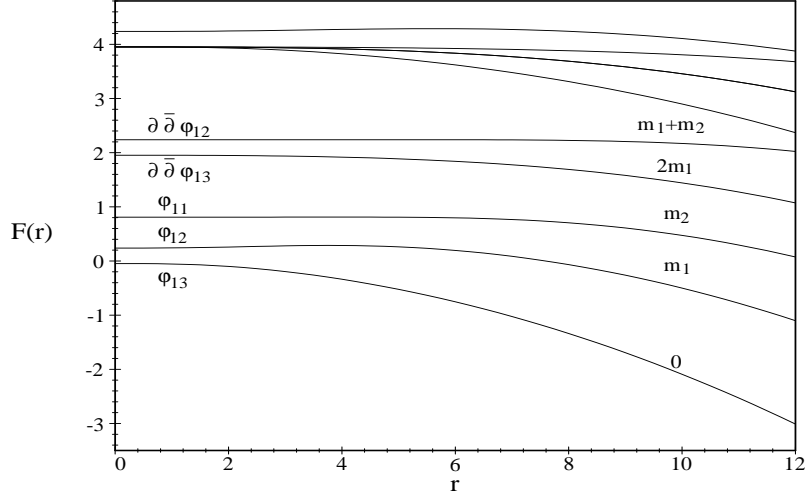


Figure 2: TCSA data for real r between 0 and 12, with the lines labelled both by the conformal fields found in the ultraviolet, and by the mass gaps exhibited as $r \rightarrow \infty$.

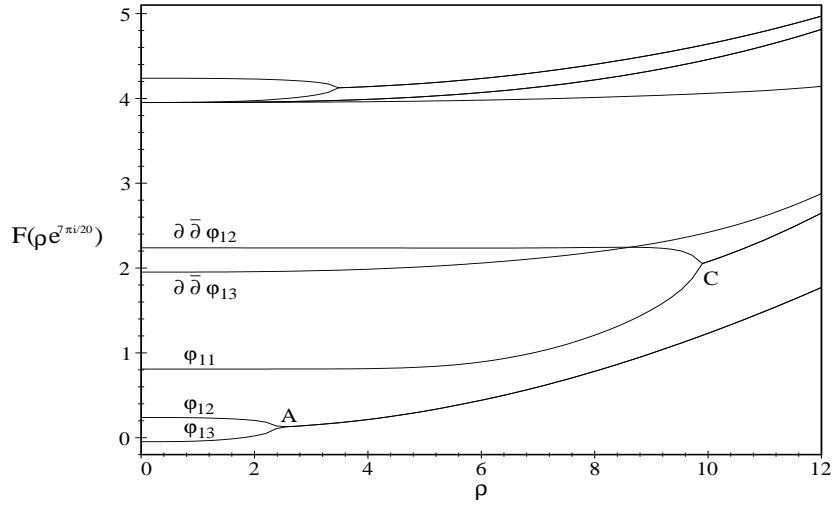


Figure 3: TCSA data for complex r on the positive- λ line $r = \rho e^{7\pi i/20}$, $0 \leq \rho \leq 12$. Three branch points can be seen; those marked A and C also appear on figure 1.

another line of interest, namely $r = \rho e^{7\pi i/20}$, $\rho \in \mathbb{R}^+$. Via equation (2.2) and the relation $r = M_1(\lambda)R$, this line also corresponds to real R and λ , but now with λ positive. Consideration of the power series expansions in λ provided by perturbed conformal field theory shows that the scaling functions must be real here too on some initial segment of the positive- λ line. Beyond the radius of convergence of the perturbative expansions singularities are found, after which the $F(r)$ can pick up imaginary parts. Examples of singularities on the positive- λ line are the branch points marked A and C in figures 1 and 3.

As noted in [5], another consequence of the perturbative series is that all other branch points occur in pairs r, \tilde{r} , related by a complex conjugation of λ , which reflects the complex r -plane in the positive- λ line. This parallels the involution of the Y 's discussed at the end of the last section. For $N=2$, the relationship is

$$\tilde{r} = e^{7\pi i/10} r^* . \quad (3.1)$$

Examples in figure 1 are the pairs B, \tilde{B} ; D, \tilde{D} ; and E, \tilde{E} .

Using the branch points, it is possible to move between the energy levels. A path encircling A will link the ground state with the first excited state, one encircling A and then B will link the ground state with the second excited state, and so on. During this continuation, singularities in one or other of L_1 and L_2 may cross the real axis. Whenever this happens, all integration contours in the TBA equations must be distorted to run around these singularities. When the contours are returned to the real axis, residue terms are picked up, resulting in modified equations in which the positions of some singularities make an explicit appearance. We will call these singularities 'active', and the others 'inactive'.

This was described for the case of the SLYM in [5]. The principles are the same here, but the practice is considerably more complicated, and the rest of this section will be devoted to a detailed description of how it goes for the cases of zero, one and two pairs of active singularities (note, the $\theta \rightarrow -\theta$ symmetry of the initial TBA means that singularities always either appear or disappear from the equations in pairs). It will sometimes be convenient to use the functions $z_a(\theta)$, $a = 1, 2$, where

$$z_a(\theta) = 1 + e^{-\varepsilon_a(\theta)} = 1 + Y_a(\theta)^{-1} .$$

Singularities of $L_a(\theta) = \log z_a(\theta)$ are found at zeroes and poles of z_a , where Y_a takes the values -1 and 0 respectively. It will be important later that these singularities never come singly: the T_2 Y-system (2.5) ties together

the values of the $Y_a(\theta)$ at locations separated by integer multiples of $i\pi/5$. We will label the zeroes of $Y_1(\theta)$ as $\pm\beta_2^{(j)}$, $j = 0 \dots \infty$. With each zero, the following other special values are forced:

k	...	-1	0	1	...	
$Y_1(\beta_2^{(j)} + \frac{ik\pi}{5})$...	y	0	$1/y$...	(3.2)
$Y_2(\beta_2^{(j)} + \frac{ik\pi}{5})$...	-1	0	-1	...	

Here y is free, although it should not be zero since, as mentioned earlier, Y_1 and Y_2 are expected to be entire functions of θ . The zeroes of $Y_2(\theta)$ occur either at the points $\pm\beta_2^{(j)}$ already captured in the above table, or else at a further set of points $\pm\beta_1^{(j)}$, which entail a different singularity pattern:

k	...	-1	0	1	...	
$Y_1(\beta_1^{(j)} + \frac{ik\pi}{5})$...	-1	a	-1	...	(3.3)
$Y_2(\beta_1^{(j)} + \frac{ik\pi}{5})$...	y	0	$(1+a)/y$...	

This time both y and a are nonzero (the latter condition preventing singularities in some of the omitted terms in the table).

As for the other type of singularity in $L_a(\theta)$, corresponding to a zero of $z_a(\theta)$ with $Y_a(\theta) = -1$, it is not hard to check that $z_2(\theta) = 0$ forces (3.2), with $\beta_2^{(j)}$ equal to either $\theta - i\pi/5$ or $\theta + i\pi/5$, while $z_1(\theta) = 0$ leads to (3.3), this time with $\beta_1^{(j)}$ equal to either $\theta - i\pi/5$ or $\theta + i\pi/5$. This is the reason for the at-first-sight perverse labelling: for the analytic continuation of the TBA equations, it is the zeroes of the $z_a(\theta)$, located at $\beta_a^{(j)} \pm i\pi/5$, that turn out to play the crucial role.

To unravel the singularity structure of any particular solution, it often helps to reconstruct its ‘history’ through the analytic continuation, remembering the $\theta \rightarrow -\theta$ symmetry of the equations. Also useful are the facts that whenever r is real, the singularity pattern must additionally be symmetrical under the standard conjugation $\theta \rightarrow \theta^*$, and that whenever r lies on the positive- λ line, so that $\tilde{r} = r$ in (2.10), the pattern is either symmetrical under the shifted conjugation $\theta \rightarrow \tilde{\theta}$, or else is mapped by this operation onto the pattern for another solution \tilde{Y}_a .

For later use, we will record the situation for the solutions to the basic TBA equation (2.3), when r is real. A typical pattern, in fact that found at $r=1$, is shown in figure 4. The points $\pm\beta_a^{(j)}$ all have imaginary parts equal

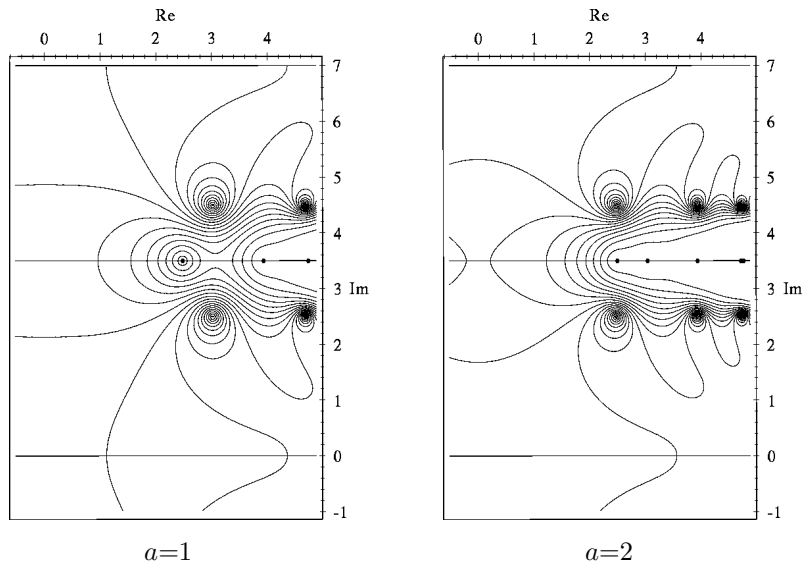


Figure 4: Contour plots of $|z_a(\theta)/(1+|z_a(\theta)|)$ in the complex θ plane, for the basic TBA equation with $r=1$. Concentric patterns of contours are signs of singularities in $L_a(\theta)$. Those corresponding to zeroes of $Y_a(\theta)$ are marked by dots \bullet ; the others are zeroes of $z_a(\theta)$. The scales on the axes are in units of $\pi/5$.

to $7\pi/10$ (the same, by the periodicity (2.6), as $-7\pi/10$), and so all of the zeroes of Y_1 and Y_2 lie on the line $\text{Im } \theta = \pm 7\pi/10$. The zeroes of z_1 and z_2 , as follows from (3.3) and (3.2) respectively, lie on the lines $\text{Im } \theta = \pm\pi/2$. For definiteness, we will choose the β 's to have negative real parts, and to be ordered from left to right:

$$\dots < \text{Re } \beta_a^{(j)} < \text{Re } \beta_a^{(j-1)} < \dots < \text{Re } \beta_a^{(0)} < 0. \quad (3.4)$$

As $r \rightarrow 0$, solutions to TBA equations of this sort split into pairs of 'kink systems'. One starts near $-\log(1/r)$ and runs leftwards, the other starts near $+\log(1/r)$ and runs rightwards, and in the region between the two the pseudoenergies are approximately constant. With the labelling choice just adopted, the zeroes of Y_1 and Y_2 in the left-hand system are at $\{\beta_2^{(i)}\}$ and $\{\beta_2^{(i)}, \beta_1^{(j)}\}$ respectively, and those of the right-hand system are at $\{-\beta_2^{(i)}\}$ and $\{-\beta_2^{(i)}, -\beta_1^{(j)}\}$. Thus the singularities visible in figure 4 all belong to the developing right-hand kink system, and move further to the right as r

decreases.

In the deep ultraviolet, the mutual interaction of the two kink systems becomes vanishingly small, and they separately solve kink forms of the TBA equations, obtained by replacing every occurrence of $r \cosh \theta$ either by $\frac{1}{2}re^{-\theta}$ (for the left-hand kink system) or by $\frac{1}{2}re^{\theta}$ (for the right-hand system). In the kink forms of the equations, the dependence on r is trivial: any further changes can be absorbed by a compensating shift in θ . This tells us something new about the singularity locations in this limit: the singularities in the left-hand set are at fixed distances from the point $\theta = -\log(1/r)$, while those in the right-hand set are oppositely placed, at fixed distances from the point $\theta = \log(1/r)$. To make this more precise, we have

$$\lim_{r \rightarrow 0} \left[\beta_a^{(j)} + \log(1/r) \right] = c_a^{(j)} , \quad (3.5)$$

with $\{c_a^{(j)}\}$ a set of constants satisfying $\text{Im } c_a^{(j)} = \pm 7\pi/10$. At large j , the real parts of the $c_a^{(j)}$ are given by

$$\text{Re } c_a^{(j)} \sim -\log \left(\frac{2}{m_a} (2j+1)\pi \right) \quad (j \gg 1) .$$

For smaller j these real parts are somewhat distorted, though the counting (starting at $j = 0$) is correctly given by this formula.

During analytic continuation, the singularities will move around, and for most of the time we will use the same labels for the singularities of the continued solutions. To avoid ambiguity we must remember the particular path in the complex r -plane chosen to reach a given solution, since there are closed paths on the Riemann surface around which pairs of singularities swap over. Some examples will be seen later.

3.1 The basic TBA in the complex plane

This case provides the starting-point for the investigation. If r is continued up from the real axis onto the positive- λ line, then a function $F(\rho e^{7\pi i/20})$ is obtained, from the basic TBA equations (2.3) and (2.4), which is real out to $\rho = \rho_0 = 2.39342(4)$. This point matches the branch point A found from the TCSA. On this segment Y_1 and Y_2 are self-conjugate in the shifted sense of equations (2.10) and (2.11):

$$Y_a(\rho e^{7\pi i/20}, \theta) = Y_a^*(\rho e^{7\pi i/20}, \tilde{\theta}), \quad 0 \leq \rho \leq \rho_0 . \quad (3.6)$$

This means that the singularities in L_1 and L_2 are arranged symmetrically with respect to the shifted conjugation $\theta \rightarrow \tilde{\theta} = 7\pi i/10 + \theta^*$. Here this

happens in the simplest possible way, with the zeroes of Y_1 and Y_2 lying on the fixed lines of the mapping, $\text{Im } \theta = \pm 7\pi/20$, and the zeroes of the z 's symmetrically arranged on the lines $\text{Im } \theta = \pm 3\pi/20$ and $\text{Im } \theta = \pm 11\pi/20$. All zeroes in the left half-plane, with negative real parts, lie on the lower triplet of lines, and all to the right lie on the upper triplet. Figure 5 shows the situation at $|r| = \rho = 1$. Given the symmetry (3.6), the zeroes must

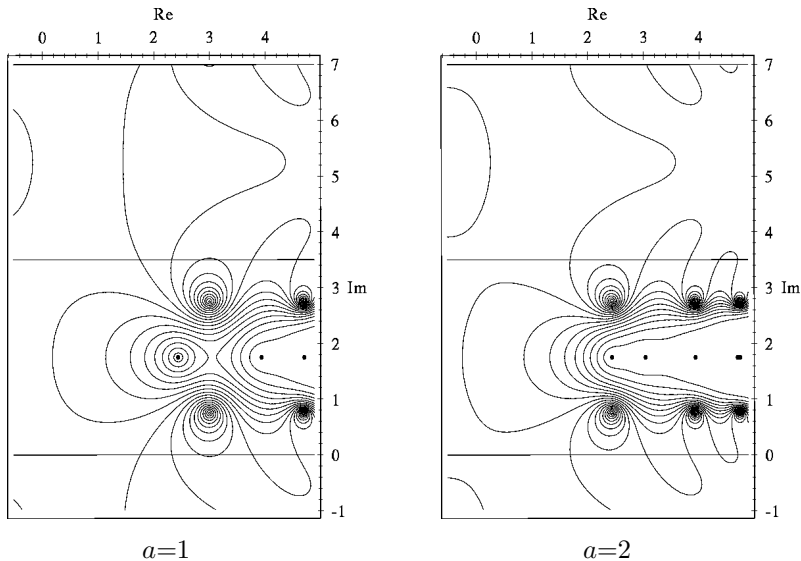


Figure 5: Contour plots of $|z_a(\theta)|/(1+|z_a(\theta)|)$ in the complex θ plane, for the ground-state solution to the basic TBA equation with $r=e^{7\pi i/20}$, $\rho=1$. Labelling as in figure 4.

lie *exactly* on the lines just described, if they are not to be doubled up. A similar phenomenon was observed in [5] for the SLYM, although at the time it was not understood in terms of the shifted conjugation symmetry, and so was only verified numerically. Such a check was also carried out here, confirming expectations to a precision of 15 digits along the whole segment $0 < \rho < \rho_0$, and then showing the singularities moving away with a square-root type behaviour as ρ passed ρ_0 and the solutions ceased to be self-conjugate.

In the ultraviolet limit, $\rho \rightarrow 0$, the splitting into kink systems occurs just as for real values of r . Using the result (3.5) for the asymptotic singularity positions, equally valid for these complex values of r , it is easily seen how the

singularities move during the continuation from the real axis to the positive- λ line. For example, the zeroes of Y_1 and Y_2 in the left-hand system move up from the line $\text{Im } \theta = -7\pi/10$ to sit on the line $\text{Im } \theta = -7\pi/20$, while those in the right-hand set move down from $\text{Im } \theta = +7\pi/10$ to $\text{Im } \theta = +7\pi/20$. (If we had instead continued r down into the lower half-plane, these motions would have been reversed.) Comparing figures 4 and 5 should clarify the relationship between the patterns before and after continuation up onto the positive- λ line.

Of the zeroes of the $z_a(\theta)$, those at $\pm(\beta_a^{(j)} + i\pi/5)$ now lie closest to the real axis, and will be the most important later. Hence we define

$$\theta_a^{(j)} = \beta_a^{(j)} + i\pi/5 .$$

This was for the ground-state solution to the basic TBA equation. But there is another solution to this equation on the segment of the positive- λ line between $\rho = 0$ and $\rho = \rho_0$. This can be obtained by continuing the solution already discussed anticlockwise around the point $r = \rho_0 e^{7\pi i/20}$. In the process, no singularities in $L_1(\theta)$ or $L_2(\theta)$ cross the real axis and so no modifications to the TBA equation (2.3) are required. However the pseudoenergies undergo a nontrivial monodromy, and on evaluating the integrals in (2.4), a different answer is found which matches perfectly with the first excited state on the segment $0 \leq \rho \leq \rho_0$, which is the line labelled by φ_{12} in figure 3.

During the anticlockwise continuation of the ground-state solution, $\theta_2^{(0)}$, the rightmost zero of $z_2(\theta)$ in the left-hand kink system, migrates across to join the right-hand system, while the matching zero in the right-hand system makes the opposite journey. The final pattern again respects the $\theta \rightarrow \tilde{\theta}$ symmetry, but now with a different distribution for the imaginary parts of the singularities between the left and right kink systems. The change in the pattern of singularities can be appreciated on comparing figure 6, which shows the new excited solution on the positive- λ line at $\rho=1$, with figure 5, the ground-state solution at the same value of ρ .

The movement of singularities as the point $\rho = \rho_0$ is approached along the positive- λ line is shown in figure 7, which plots the real parts of $\theta_1^{(0)}$ and $\theta_2^{(0)}$ against $\log(1/\rho)$, both for the ground state and for the first excited state. The slopes tend to ± 1 as $\rho \rightarrow 0$, the slopes of -1 being characteristic of members of the left-hand kink system, and the slope of $+1$ acquired by the ‘excited’ zero of $z_2(\theta)$ showing that it has joined the right-hand kink system.

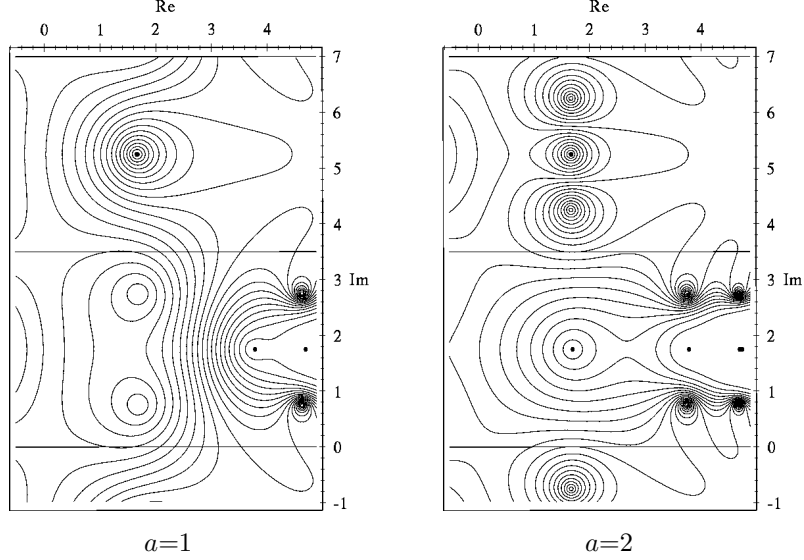


Figure 6: Contour plots of $|z_a(\theta)|/(1+|z_a(\theta)|)$ in the complex θ plane, for the excited solution to the basic TBA equation with $r=e^{7\pi i/20}$, $\rho=1$. Labelling as in figure 4.

Equation (3.5) must be modified to take account of the defection of the two singularities, one from left to right and the other from right to left. To prepare for more general situations, which may involve further pairs of defectors, we replace (3.5) by

$$\lim_{|r| \rightarrow 0} \left[\nu_a^{(j)} \beta_a^{(j)}(r) + \log(1/r) - c_a^{(j)} \right] = 0, \quad (3.7)$$

where $\nu_a^{(j)}$ is $+1$ if the singularity at $\beta_a^{(j)}$ is still part of the left-hand kink system, but switches to -1 if it has joined the right-hand system. The values of the constants $c_a^{(j)}$ are characteristic of each particular kink solution, while the $\nu_a^{(j)}$ preserve some memory of how the solution has been obtained by continuation from the ground state. For example, it appears that only for the ground state do all of the $c_a^{(j)}$ have imaginary parts equal to $\pm 7\pi/10$. For the excited state now under discussion, $\text{Im } c_2^{(0)}$ has become equal to zero, and $\nu_2^{(0)}$ is equal to -1 .

It is instructive to see how the analytic treatment of the ultraviolet limit must be modified to cope with this excited solution to the basic TBA. The

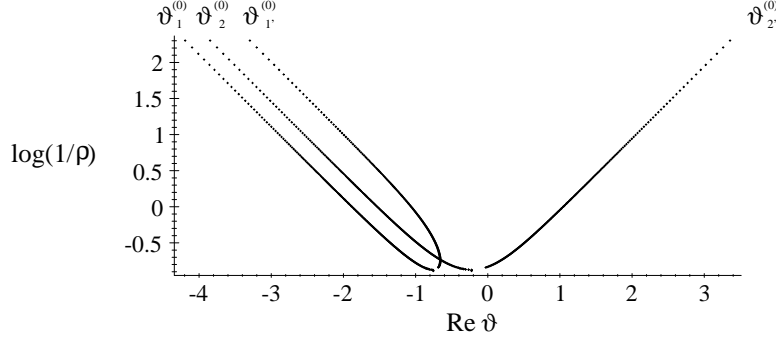


Figure 7: Real parts of $\theta_1^{(0)}$ and $\theta_2^{(0)}$ for r on the positive- λ line, plotted against $\log(1/\rho)$. The lines marked $\theta_1^{(0)}$ and $\theta_2^{(0)}$ are for the ground-state solution, and those marked $\theta_1^{(0)'}$ and $\theta_2^{(0)'}$ are for the excited state.

usual manipulations of the kink forms of equations (2.3) and (2.4) give

$$c(0) = \frac{6}{\pi^2} \sum_{a=1}^2 L_+(\mathcal{C}_a) \quad (3.8)$$

where, borrowing some notation from of refs. [15] and [16],

$$L_+(\mathcal{C}_a) = \frac{1}{2} \int_{\mathcal{C}_a} \left[\frac{\text{Log}_{\mathcal{C}_a}(1+x)}{x} - \frac{\text{Log}_{\mathcal{C}_a}(x)}{1+x} \right] dx . \quad (3.9)$$

The \mathcal{C}_a are certain contours in the complex plane, and $\text{Log}_{\mathcal{C}_a}(z)$ stands for a continuous branch of $\log(z)$ along the contour \mathcal{C}_a ; the starting-point of the branch will be determined shortly. The modification to the ground-state value of $c(0)$ resides in the form of these contours and branches, and care must be taken to identify them correctly. The variable change leading to (3.8) tells us that the contour \mathcal{C}_a in (3.9) is given by $x(\theta) = \exp(-\varepsilon_a^{\text{kink}}(\theta))$, with θ real and running from $+\infty$ (at the start of the contour) to $-\infty$ (at the end), and $\varepsilon_a^{\text{kink}}(\theta)$ the (excited) kink solution to the TBA equation. As $\theta \rightarrow \infty$, all pseudoenergies diverge and hence the contours \mathcal{C}_a always start at the origin. In the opposite direction, the kink pseudoenergies tend to finite constants and as a result the contours terminate at points $x_a = 1/Y_a$, with the constants (Y_1, Y_2) providing a stationary (θ -independent) solution to the $N=2$ case of the Y-system (2.5):

$$Y_1^2 = (1 + Y_2),$$

$$Y_2^2 = (1 + Y_1)(1 + Y_2). \quad (3.10)$$

There are four solutions to this equation: one, $(Y_1, Y_2) = (-1, 0)$, appears not to be relevant (it would anyway require $\varepsilon_2 = -\infty$), whilst the others can be written as $(Y_1, Y_2) = (y_1^{(s)}, y_2^{(s)})$ with $s = 1, 3, 5$, and

$$y_a^{(s)} = \frac{\sin(sa\pi/7) \sin(s(a+2)\pi/7)}{\sin(s\pi/7)^2}. \quad (3.11)$$

These numbers feature in certain sum rules for dilogarithm functions. When the dust has settled, it will be most convenient to have these written in terms of the Rogers dilogarithm $\mathcal{L}(y)$, defined for real y in the unit interval by

$$\mathcal{L}(y) = -\frac{1}{2} \int_0^y dt \left(\frac{\log(1-t)}{t} + \frac{\log t}{1-t} \right). \quad (3.12)$$

(In cases when \mathcal{C}_a runs from 0 to x along the real axis, with all logarithms in (3.9) on their principal branches, $L_+(\mathcal{C}_a) = \mathcal{L}(x/(1+x))$.) The sum rules that we shall need are the following:

$$\mathcal{L}\left(\frac{1}{1+y_1^{(1)}}\right) + \mathcal{L}\left(\frac{1}{1+y_2^{(1)}}\right) = \frac{4}{7} \frac{\pi^2}{6} \quad (3.13)$$

$$-\mathcal{L}\left(1+y_1^{(3)}\right) - \mathcal{L}\left(1+y_2^{(3)}\right) = -\frac{6}{7} \frac{\pi^2}{6} \quad (3.14)$$

$$\mathcal{L}\left(\frac{1}{1+y_1^{(5)}}\right) - \mathcal{L}\left(1+y_2^{(5)}\right) = \frac{2}{7} \frac{\pi^2}{6} \quad (3.15)$$

Note that all of the arguments have been adjusted so as to lie in the interval $[0, 1]$. There do exist prescriptions to extend the Rogers dilogarithm beyond this range, but at this stage it is better for us to keep our options open, since the relevant continuations will anyway be determined by the TBA equations.

For the ground state there is an additional physical requirement that the Y 's be positive and the logarithms real, and this selects the $s=1$ solution and, via (3.13), the expected result $c(0) = 4/7$ is recovered. For excited states there are no such constraints, and for the state under discussion here, $s=3$. This can be justified either by an appeal to numerical results at small $|r|$, or else by noticing that, as a result of the shifted conjugation symmetry, the functions $Y_a^{\text{kink}}(\theta) = \exp(\varepsilon_a^{\text{kink}}(\theta))$ are real along the line $\text{Im } \theta = 21\pi/20$, and that they each have a single zero on this line, at $\beta_2^{(0)}$. Since as $\theta \rightarrow \infty$

both are positive (tending to $+\infty$), they must both be negative at $\theta = -\infty$, and this picks out the $s=3$ solution.

The contours \mathcal{C}_1 and \mathcal{C}_2 join the origin to the points x_1 and x_2 respectively, avoiding the singularity at $x = -1$ (note that both x_1 and x_2 are less than -1 for this solution). Examining numerically the small- $|r|$ behaviour of the full TBA equation, we found that the correct path to take loops under $x = -1$ for \mathcal{C}_1 , and over $x = -1$ for \mathcal{C}_2 .

Finally, we should settle the branches of the logarithms. The branches of the $L_a(\theta)$ in the TBA are such that $L_a(+\infty) = 0$ (otherwise, the integral (2.4) would make no sense). This translates into the branch of $\text{Log}_{\mathcal{C}_a}(1+x)$ being such that this function is zero at $x = 0$. From this and the way that the two contours go round the point $x = -1$ follows the behaviour at the other ends of the contours:

$$\begin{aligned}\text{Log}_{\mathcal{C}_1}(1+x_1) &= \log|1+x_1| - i\pi; \\ \text{Log}_{\mathcal{C}_2}(1+x_2) &= \log|1+x_2| + i\pi.\end{aligned}\tag{3.16}$$

(Here and below, $\log x$ stands for the single-valued branch of the logarithm, with $\text{Im } \log x \in (-\pi, \pi]$.) The branch of $\text{Log}_{\mathcal{C}_a} x$ can now be determined from the stationary form of the kink TBA equation:

$$\varepsilon_a^{\text{kink}}(-\infty) = \sum_{b=1}^2 N_{ab} L_b^{\text{kink}}(-\infty)\tag{3.17}$$

where

$$N_{ab} = -\frac{1}{2\pi} \int_{-\infty}^{\infty} \phi_{ab}(\theta) d\theta = \begin{pmatrix} 1 & 2 \\ 2 & 3 \end{pmatrix}_{ab}.\tag{3.18}$$

Taking the imaginary part of (3.17), and using the relations $\text{Log}_{\mathcal{C}_a}(x_a) = -\varepsilon_a^{\text{kink}}(-\infty)$ and $\text{Log}_{\mathcal{C}_a}(1+x_a) = L_a^{\text{kink}}(-\infty)$, gives

$$\begin{aligned}\text{Log}_{\mathcal{C}_1}(x_1) &= \log|x_1| - i\pi; \\ \text{Log}_{\mathcal{C}_2}(x_2) &= \log|x_2| - i\pi.\end{aligned}\tag{3.19}$$

Now $c(0)$ can be calculated, using the strategy advocated in ref. [17]. First deform \mathcal{C}_1 and \mathcal{C}_2 to run along the negative real x axis, save for a small semicircle below -1 for \mathcal{C}_1 , and a small semicircle above -1 for \mathcal{C}_2 . The contours can then be split into segments and the integrands reexpressed in terms of the single-valued logarithm $\log x$, always with positive real arguments. For $L_+(\mathcal{C}_1)$ this goes as follows. We have

$$2L_+(\mathcal{C}_1) = A - B$$

with

$$\begin{aligned}
A &= \int_{\mathcal{C}_1} \frac{\text{Log}_{\mathcal{C}_1}(1+x)}{x} dx \\
&= \int_0^{-1} \frac{\log(1+x)}{x} dx + \int_{-1}^{x_1} \frac{\text{Log}_{\mathcal{C}_1}(1+x)}{x} dx \\
&= \int_0^1 \frac{\log(1-x)}{x} dx + \int_{-1}^{x_1} \frac{\log(-1-x)}{x} dx - \int_{-1}^{x_1} \frac{i\pi}{x} dx \\
&= \int_0^1 \frac{\log(1-x)}{x} dx + \int_0^{-x_1-1} \frac{\log x}{x+1} dx - i\pi \log(-x_1)
\end{aligned}$$

and

$$\begin{aligned}
B &= \int_0^{x_1} \frac{\text{Log}_{\mathcal{C}_1}(x)}{1+x} dx \\
&= \int_0^{x_1} \frac{\log(-x)}{1+x} dx - \int_0^{x_1} \frac{i\pi}{1+x} dx \\
&= - \int_0^1 \frac{\log x}{1-x} dx - \int_0^{-x_1-1} \frac{\log(1+x)}{x} dx - \pi^2 - i\pi \log(-1-x_1).
\end{aligned}$$

(In the second calculation, any integrals from 0 to x_1 should be understood as including the small semicircle below -1 .) Collecting the pieces together and dividing by 2, the final result for $L_+(\mathcal{C}_1)$ is

$$L_+(\mathcal{C}_1) = -\mathcal{L}(1) - \mathcal{L}(1 + 1/x_1) + \pi^2 + i\pi \log [(1+x_1)/x_1] .$$

The calculation of $L_+(\mathcal{C}_2)$ is similar, save for the switch to $\text{Log}_{\mathcal{C}_2}$ and the fact that the semicircular part of the contour must now go above the point $x = -1$ instead of below it, causing $+\pi^2$ to be replaced by $-\pi^2$. Adding everything together,

$$\sum_{a=1}^2 L_+(\mathcal{C}_a) = - \sum_{a=1}^2 (\mathcal{L}(1) + \mathcal{L}(1+1/x_a)) + \frac{i\pi}{2} \log [(1+x_1)(1+x_2)x_2/x_1] .$$

The stationary Y-system, satisfied by the $1/x_a$, can be used to show that the argument of the logarithm is equal to 1, and hence the imaginary part of the sum vanishes. For the rest, substituting $x_a = 1/y_a^{(3)}$, and using $\mathcal{L}(1) = \pi^2/6$, and the sum rule (3.14), gives

$$c(0) = -20/7,$$

which is the expected answer.

3.2 Singular lines and branch points

The basic TBA continues to apply so long as none of the singularities of L_1 or L_2 touch the real axis. To put this consideration into a more general setting, imagine that the full Riemann surface covering the complex r plane is marked with a set of lines, along each of which a given singularity in L_1 or L_2 has a vanishing imaginary part. As one of these ‘singular lines’ is crossed, singularities change their status from inactive to active or vice versa, and a transition is induced in the TBA equations. There is a distinction to be made between the two different types of singularity that the $L_a(\theta)$ can have, one stemming from $z_a(\theta) = 0$, the other from $Y_a(\theta) = 0$. Transitions associated with the zeroes of the $z_a(\theta)$ always result genuinely different TBA equations, and we will refer to the corresponding singular lines as being of ‘type I’. The same turns out not to be true of the transitions associated with zeroes of the $Y_a(\theta)$, and these singular lines will be called ‘type II’. Further discussion of this point will be delayed until section 3.4, when a concrete example will be examined.

It is important to realise that these singular lines are associated with transitions at the level of the TBA equations, and *not* with singular behaviour of the Y ’s as functions of r , still less with singular behaviour of the scaling functions. For example, if we had chosen to set up the TBA equations using a contour other than the real axis for all of the integrations, then the set of lines across which equations changed from one form to another would have been differently placed. Nevertheless, the singular lines do provide an effective way to map the full Riemann surface, and they are also very useful as a means to organise the various generalised TBA equations. However, even for a model as simple as the one under consideration here, it is by no means an easy task to find their pattern. The main problem is that at a point on the Riemann surface near to a singular line, a singularity in L_1 or L_2 will inevitably be near to the real θ axis, and this tends to destabilise the iteration schemes used to solve the equations. This makes it rather hard to disentangle the genuine boundary of applicability of a given equation from its ‘region of stability’, the latter region depending on the particular numerical method employed and therefore having no intrinsic interest. One technique to get around this difficulty is to locate the singularity positions with high accuracy in those regions where iteration does work well, and then to extrapolate these positions into the ‘difficult’ regions around the singular lines. Especially in situations where data can be obtained on both sides of a given line, this allows its location to be found with a fair degree

of confidence. However the method is distinctly tedious to implement, and there is always the possibility that a crucial singularity has been missed. In some cases, it is possible to do much better. The key idea is to make use of the shifted conjugation property (2.11). If a singularity in $L_a(r, \theta)$ crosses the real axis, the corresponding point for $\tilde{L}_a(\tilde{r}, \theta)$ will be crossing the line $\text{Im } \theta = 7\pi/10$, a harmless piece of behaviour from the point of view of the equations for $\tilde{\varepsilon}_a$. This makes it possible to find the functions Y_a at many points where the direct attempt at numerical solution of the relevant TBA fails, simply by solving the equations for \tilde{Y}_a instead.

This remark can be put to immediate use, to resolve an apparent paradox about the behaviour of the solutions discussed so far in the neighbourhood of the point $\rho=\rho_0$ on the positive- λ line. Recall that along the initial segment of the positive- λ line, the singularities of the $L_a(\theta)$ nearest to the real axis were at $\theta = \pm\theta_a^{(j)}$, and all had imaginary parts equal to $\pm 3\pi/20$. At first sight this is puzzling: in the case of the Ising model the branch points in the scaling functions can all be associated with the ‘pinching’ of the real θ axis by pairs of colliding singularities (see [5] for a discussion), and yet here, as we approach the point $\rho=\rho_0$ at which there is a branch point in $c(r)$, the singularities in L_1 and L_2 show no inclination at all to pinch the real axis. The resolution is rather appealing: the interacting nature of this model as compared to Ising, reflected in the fact that a TBA equation must be solved before the pseudoenergies can be found, serves to ‘desingularise’ the pinch. Instead, in the immediate vicinity of $\rho=\rho_0$, the branching of $c(r)$ is due entirely to the multivalued nature of the solutions to the basic TBA equation. Get a little further away, and singularities start to cross the real axis as the point $\rho=\rho_0$ is encircled, making the analysis similar to that of a pinch singularity. This fact, coupled to the severe instability of the ‘excited’ solution near to the branch point, makes it easy to confuse the situation with a genuine pinch singularity. However, with the help of the conjugation trick just described, the numerical problems can be circumvented and the ambiguity resolved. We first observe that as ρ increases beyond ρ_0 , the functions $Y_a(\theta)$ found from ground-state solution to the basic TBA cease to be self-conjugate. Hence the conjugated functions $\tilde{Y}_a(\theta)$ start to differ from the $Y_a(\theta)$, and provide alternative solutions to some set of TBA equations. For $\rho_0 < \rho < 2.8$, none of the singularities in $\tilde{L}_1(\theta)$ and $\tilde{L}_2(\theta)$ have crossed the real θ axis, and so the $\tilde{\varepsilon}_a(\theta)$ continue to solve the basic TBA equation, rather than one of its generalisations. We used these functions in (2.4) to find a scaling function in the segment $\rho_0 < \rho < 2.8$ of the positive- λ line,

with results which matched perfectly with the energy level missed by the ground-state solution. (Note that while the two levels appear to sit on top of each other for $\rho > \rho_0$ on figure 3, this is an illusion caused by the equality of their real parts – the imaginary parts are different.) Moving beyond $\rho = 2.8$, pairs of singularities in the conjugated functions (first in \tilde{L}_2 , and then, at around $\rho = 4.2$, in \tilde{L}_1) cross the real axis and the basic TBA together with the conjugation trick provides us, for free, with solutions to a couple of generalised TBA equations.

In the ultraviolet limit, that is in those regions of the Riemann surface covering the neighbourhood of the point $r=0$, another simple observation constrains the pattern of singular lines rather strongly. The idea is to exploit the control over the ultraviolet singularity positions given to us by the splitting into kink systems, and the consequent formula (3.7). This information can be used in the following way. Since $\log(1/r) = \log(1/|r|) - i \arg(r)$, changing the modulus of r , once the kink systems have formed, does not affect the imaginary parts of the singularity locations. However, a change in the value of $\arg(r)$ does have an effect, and may result in a singularity hitting the real θ axis. Once this has happened, varying $|r|$ again, while holding $\arg(r)$ fixed, just slides this singularity along the real axis without shifting its imaginary part away from zero. Hence the asymptotic pattern of the singular lines near to the origin is a collection of rays emanating from $r=0$. Their directions follow from (3.7): for the type I lines, associated with zeroes of $z_a(\theta)$, they are

$$\arg(r) = \pm \left(\text{Im } c_a^{(j)} \pm \frac{\pi}{5} \right) \quad (3.20)$$

while for the type II lines, associated with zeroes of $Y_a(\theta)$, the relevant directions are

$$\arg(r) = \pm \text{Im } c_a^{(j)} . \quad (3.21)$$

For the ground state pseudoenergies solving the basic TBA equation, all of the $c_a^{(j)}$ have imaginary parts equal to $7\pi/10$. It follows that there are no singular lines approaching the origin in the sector $-\pi/2 \leq \arg(r) < \pi/2$ of the first sheet of the Riemann surface. However for the excited solution, which was initially discussed only on the positive- λ line $\arg(r) = 7\pi/20$, we saw that $\text{Im } c_2^{(0)}$ vanished, and so (3.20) implies that a type I singular line approaches the origin on the second sheet along $\arg(r) = \pi/5$. As this line is traversed, a zero of $z_2(\theta)$ crosses the real axis and the pseudoenergies start to be determined by the first generalised TBA equation, to be discussed

shortly. In fact we already know a kink solution to this equation: it is just the excited kink solution to the basic TBA, shifted yet further in the imaginary θ direction as appropriate for the diminishing value of $\arg(r)$. To find out what happens to this solution as the ultraviolet region is left, we now turn to a direct analysis of the generalised TBA equation that it solves.

3.3 One pair of active singularities

As r crosses the type I singular line on the second sheet, the singularities in $L_2(\theta)$ at $\pm\theta_2^{(0)}$ cross the real axis, the imaginary part of $\theta_2^{(0)}$ becoming for the first time positive. Contours in integrals involving $L_2(\theta)$ must be distorted, and returning them to the real axis induces extra residue terms in the equations. Just as described in ref. [5] for the SLYM, these residues can be found via an integration by parts. Equations (2.3) and (2.4) become

$$\varepsilon_a(\theta) = m_a r \cosh \theta + \text{Log}_{\mathcal{C}} \frac{S_{a2}(\theta - \theta_2^{(0)})}{S_{a2}(\theta + \theta_2^{(0)})} - \sum_{b=1}^2 \phi_{ab} * L_b(\theta) \quad (3.22)$$

and

$$c(r) = \frac{12r}{\pi} \iota m_2 \sinh \theta_2^{(0)} + \frac{3}{\pi^2} \sum_{a=1}^2 \int_{-\infty}^{\infty} d\theta m_a r \cosh \theta L_a(\theta) \quad (3.23)$$

respectively. These equations must be handled with some care. A continuous branch of the logarithm, signalled by $\text{Log}_{\mathcal{C}}$, is implied. We set

$$\text{Log}_{\mathcal{C}} S_{ab}(+\infty) = 0 \quad ; \quad L_b(+\infty) = 0, \quad (3.24)$$

and then understand $\text{Log}_{\mathcal{C}}(S/S)$ to be continuous as θ varies along the real axis. For the moment we shall also assume $0 < \text{Im} \theta_2^{(0)} < \pi/5$; the effects of $\theta_2^{(0)}$ straying beyond this strip will be examined later. Using $\phi_{ab} = -\iota \frac{\partial}{\partial \theta} \log S_{ab}(\theta)$, we have

$$[\text{Log}_{\mathcal{C}} S_{ab}]_{-\infty}^{\infty} = \iota \int_{-\infty}^{\infty} \phi_{ab}(\theta) d\theta \equiv -2\pi \iota N_{ab} = -2\pi \iota \begin{pmatrix} 1 & 2 \\ 2 & 3 \end{pmatrix}_{ab}.$$

Given the branch choice made above, and also the symmetry of $S_{ab}(\theta)$, this implies that

$$\text{Log}_{\mathcal{C}} S_{ab}(0) = \pi \iota N_{ab} \quad ; \quad \text{Log}_{\mathcal{C}} S_{ab}(-\infty) = 2\pi \iota N_{ab}. \quad (3.25)$$

Substituting $\theta = \theta_2^{(0)}$ into (3.22), and imposing $\varepsilon_2(\theta_2^{(0)}) = i\pi$ to ensure that $z_2(\theta)$ vanishes at that point, then gives the final ingredient:

$$0 = m_2 r \cosh \theta_2^{(0)} + \pi i (N_{22} - 1) - \text{Log}_{\mathcal{C}} S_{22}(2\theta_2^{(0)}) - \sum_{b=1}^2 \phi_{2b} * L_b(\theta_2^{(0)}) . \quad (3.26)$$

The term $\pi i N_{22}$ comes from the consistent application of the branch choice (3.24) to $\text{Log}_{\mathcal{C}} S_{22}(0)$. Notice that it is equal to $3\pi i$ and *not* the πi that might at first sight have been expected – the importance of this will become apparent during the calculation of $c(0)$ below. The remaining logarithm must also be taken continuously, starting from the branch found when $\theta_2^{(0)}$ crosses the axis. This is not completely trivial, as $2\theta_2^{(0)}$ may ultimately leave the strip $|\text{Im } 2\theta_2^{(0)}| < \pi/5$, making it necessary to keep track of the sense in which the pole in $S_{22}(\theta)$ at $\theta = i\pi/5$ is encircled.

All of this makes the analytic treatment a little tricky. Perhaps surprisingly, it is much less of a problem for the numerical solution of the equations. We used the following method: start by choosing an initial value for $\theta_2^{(0)}$, and then iterate (3.22) until a solution $\varepsilon_a(\theta|\theta_2^{(0)})$ is found. At this stage the first potential difficulty arises: unless otherwise instructed, Fortran will always choose the principal (discontinuous) branch for the logarithm during these iterations, $-\pi < \text{Im } \log(S/S) \leq \pi$. But any $2\pi i$ discontinuities that this induces in the resulting functions $\varepsilon_a(\theta|\theta_2^{(0)})$ leave the values of the $L_a = \log(1 + \exp(-\varepsilon_a))$ unchanged, both in (3.22) and (3.23), and so this problem can be ignored. The functions $\varepsilon_a(\theta|\theta_j^{(0)})$ are then inserted into (3.26); the error in the initial $\theta_2^{(0)}$ will be reflected in the degree to which this equation fails to hold. Again, one might worry that Fortran will spoil things by picking the wrong branch for the logarithm; this time, we sidestepped the problem by exponentiating the equation. Once this has been done, an adeptly-chosen portion of $S_{22}(2\theta_2^{(0)})$ can be taken over to the left-hand side, and then inverted to obtain an improved estimate for $\theta_2^{(0)}$. The whole procedure is then iterated until a stable solution is found. In this way we were able to map out large areas of the complex r plane, but not, as it happens, a segment $0 < r < r_c$ of the real axis. The reason for this difficulty will be explained later, but before that we will discuss the infrared limit.

With a little practice it is not too hard to guess how the solutions will behave in this regime, but just to be sure we tracked a solution and its singularities as r varied along the line $r = 2i + (1 - 0.5i)t$, using the basic TBA (2.3) for $0.1 < t < 1.5$, and the generalisation (3.22), (3.26) for $1.5 < t < 4$.

We found that the singularity positions are indeed smoothly continued by the new equations. When r finally reaches the real axis, the singularity positions regain the standard conjugation symmetry under $\theta \rightarrow \theta^*$, as oppose to the shifted conjugation symmetry under $\theta \rightarrow \tilde{\theta}$ associated with the positive- λ line. However the way in which the symmetry is realised is rather different from the situation before any continuation, when the basic TBA equation applied and singularity pattern was as shown in figure 4. Then, all of the $\beta_a^{(j)}$ lay on a fixed line of the mapping $\theta \rightarrow \theta^*$, namely $\text{Im } \theta = 7\pi/10$. (Recall that all functions in the game are $7\pi\nu/5$ -periodic, so this is indeed a fixed line.) This time, $\beta_1^{(0)}$ and $\beta_2^{(0)}$ are instead swapped with their negatives under the conjugation; they are therefore both purely imaginary. Figure 8

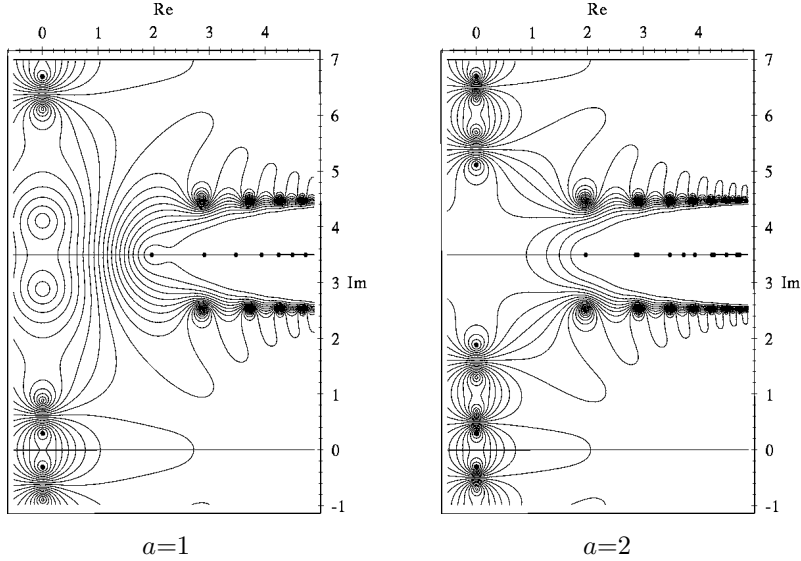


Figure 8: Contour plots of $|z_a(\theta)|/(1+|z_a(\theta)|)$ in the complex θ plane, for the first generalised TBA equation with $r=3$. Labelling as in figure 4.

shows the functions at $r = 3$; note how, in contrast to the earlier pictures, the zeroes of Y_1 and Y_2 at $\beta_1^{(0)}$ and $\beta_2^{(0)}$ (signalled by the dots \bullet on the imaginary axis) are clear of the fixed lines of $\theta \rightarrow \theta^*$ and $\theta \rightarrow \tilde{\theta}$.

Once these qualitative features have been understood, it is possible to extract some exact asymptotics. On the real axis with r larger than r_c , $\theta_2^{(0)}(r)$ lies on the segment of the imaginary θ axis between $i\pi/10$ and $i\pi/5$. Fur-

thermore, during the continuation from the ultraviolet end of the positive- λ line, $\theta_2^{(0)}$ reaches this segment from large positive values with no monodromy around the point $i\pi/10$. Combining this information with the form of $S_{22}(\theta)$ shows that, for real $r > r_c$,

$$\text{Log}_{\mathcal{C}} S_{22}(2\theta_2^{(0)}(r)) = \log S_{22}(2\theta_2^{(0)}(r)) + 2\pi i .$$

Equation (3.26) therefore becomes

$$0 = m_2 r \cosh \theta_2^{(0)} - \log S_{22}(2\theta_2^{(0)}) - \sum_{b=1}^2 \phi_{2b} * L_b(\theta_2^{(0)}) . \quad (3.27)$$

Since $S_{22}(2\theta)$ is real and positive for imaginary θ between $i\pi/10$ and $i\pi/5$, all three terms in this equation are real. As r grows, the first two terms must cancel, as the convolution term tends to zero. To achieve this, $\theta_2^{(0)}$ approaches the limiting value of $i\pi/10$, at which $S_{22}(2\theta_2^{(0)})$ has a pole. The leading behaviour of $c(r)$ follows immediately: substituting $\theta_2^{(0)} = i\pi/10$ into (3.23) and using the relation

$$m_1 = 2m_2 \sin\left(\frac{\pi}{10}\right) \quad (3.28)$$

gives $c(r) \sim -6m_1 r/\pi$, or $E(\lambda, R) \sim E_{\text{bulk}}(\lambda, R) + M_1$. This confirms that the state under discussion is a one-particle state, with mass gap M_1 . Since it also has zero momentum (the total momentum of a level is conserved under analytic continuation), it must be the first line above the ground state in figure 2. As a further check, a couple of corrections can be worked out. These should reproduce the formulae for finite-volume mass shifts found in refs.[1, 18], and summarised in appendix A. The more precise cancellation of the first two terms in (3.27) requires

$$\theta_2^{(0)}(r) \sim i \left(\pi/10 + \tan\left(\frac{3\pi}{10}\right) \tan\left(\frac{2\pi}{5}\right)^2 e^{-m_2 r \cos(\pi/10)} \right) . \quad (3.29)$$

This improved estimate for $\theta_2^{(0)}$ gives one correction, the so-called μ -term, when substituted into (3.23). A second comes on expanding $L_a(\theta)$ in (3.23), using the leading behaviour of $\varepsilon_a(\theta)$ obtained from the first two terms on the RHS of (3.22). For this correction we can set $\theta_2^{(0)} = i\pi/10$, and then use the identity

$$\frac{S_{a2}(\theta + i\frac{\pi}{10})}{S_{a2}(\theta - i\frac{\pi}{10})} = S_{a1}(\theta + i\frac{\pi}{2}) . \quad (3.30)$$

Putting these pieces together, the two leading IR corrections are

$$c(r) \sim \frac{-6r}{\pi} \left(m_1 + 2m_2 \cos\left(\frac{\pi}{10}\right) \tan\left(\frac{3\pi}{10}\right) \tan\left(\frac{2\pi}{5}\right)^2 e^{-m_2 r \cot(\pi/10)} \right. \\ \left. - \frac{1}{2\pi} \sum_{a=1}^2 \int_{-\infty}^{\infty} d\theta m_a \cosh \theta S_{1a}\left(\theta + \frac{i\pi}{2}\right) e^{-r m_a \cosh \theta} \right). \quad (3.31)$$

These agree with the expected results, as given in ref. [18].

In the opposite, ultraviolet limit the singularity pattern is rather different. As remarked earlier, once the limiting form of the excited solution to the basic TBA on the positive- λ line near to $r = 0$ is known, the fact that the only r -dependence of the kink solutions is in the $\pm \log(1/r)$ anchoring points for the left and right kink systems allows the solution to be continued back to the real axis, thereby obtaining a kink solution to the generalised TBA equations (3.22) and (3.26). Recall from just after (3.7) that for the excited solution to the basic TBA all of the $c_a^{(j)}$ had imaginary parts equal to $7\pi/10$ apart from $c_2^{(0)}$, which had an imaginary part equal to zero. Substituting into (3.7) shows that for real r the kink limit of this solution to the generalised TBA equation (3.22) has the imaginary parts of all of the $\beta_a^{(j)}(r)$ equal to $(\pm)7\pi/10$, apart from $\beta_2^{(0)}(r)$, for which $\text{Im} \beta_2^{(0)}(r) = 0$. This also holds before the kink limit is taken, since when r is real, the singularity pattern must be symmetrical about the real θ -axis. For a zero of Y to move away from a fixed line of $\theta \rightarrow \theta^*$, there would have to be a corresponding zero, with equal real part, moving in the opposite direction. This is only possible once the left and right kink systems have met. (Numerically we found that this happens at the previously-mentioned point $r = r_c \approx 2.6646510318(2)$.) Figure 9 shows the solution at $r=1$. Notice that the pattern of singularities is indeed symmetrical under $\theta \rightarrow \theta^*$, but in a different way from the infrared solution shown in figure 8. The situation is similar to that observed for the first excited state of the SLYM in refs. [4, 5]: as r increases from the ultraviolet, the two kink systems come into contact and the TBA profits from the extra possibilities that this offers for satisfying the conjugation symmetry, and rearranges the singularity pattern into a form more appropriate for the infrared limit. For real $r < r_c$ we have $\text{Re} \beta_2^{(0)} \neq 0$ and $\text{Im} \beta_2^{(0)} = 0$, while for real $r > r_c$, $\text{Re} \beta_2^{(0)} = 0$ and $\text{Im} \beta_2^{(0)} \in (-\pi/5, 0)$. (There is also a transition associated with $\beta_1^{(0)}$, when it moves from the line $\text{Im} \beta_1^{(0)} = 7\pi/10$ onto the imaginary axis. This happens at $r \approx 1.5$, but since the associated singularities are inactive, the equations do not change.) The transition at $r=r_c$ will

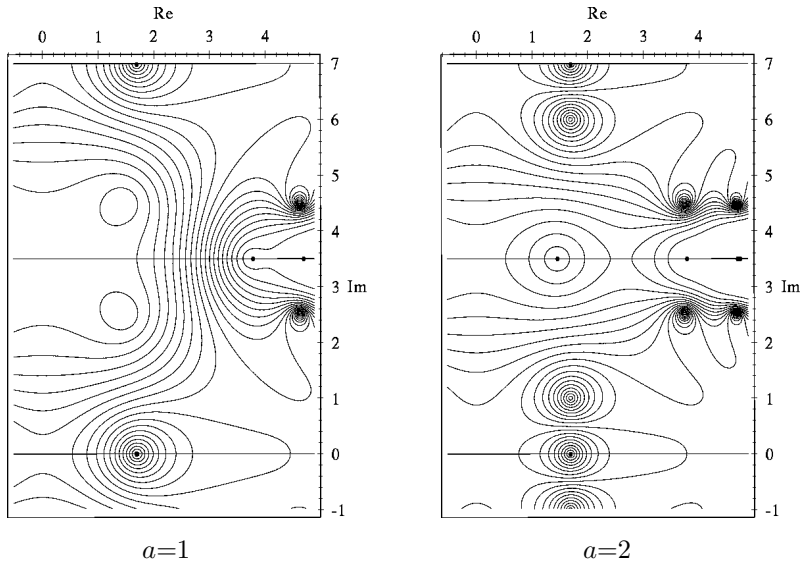


Figure 9: Contour plots of $|z_a(\theta)/(1+|z_a(\theta)|)$ in the complex θ plane, for the generalised TBA equation with $r=1$. Labelling as in figure 4.

be analysed further below, but first we will discuss the ultraviolet behaviour of the equations, where the singularities follow the pattern predicted by the excited solution to the basic TBA equation.

There is a new complication in the ultraviolet regime when r is real. Since $\beta_2^{(0)}$ is real, (3.2) implies that singularities at $\pm\beta_2^{(0)}$ in L_1 and L_2 are sitting exactly on the integration contour. For analytic work, the most convenient approach seems to be to take these singularities into account via small distortions of all contours of integration, below the real axis near to $\theta = -\beta_2^{(0)}$, and above the real axis near to $\theta = \beta_2^{(0)}$. This is rather like the usual ‘ $i\epsilon$ ’ prescription in quantum field theory, and amounts to giving r an infinitesimal positive-imaginary part. Here, the justification for the prescription comes from the analytic continuation idea that has been fundamental from the outset. (In ref. [5], we instead rewrote the equations using principal values for all integrals. Whilst this puts the equations into an appealingly symmetrical form, the branches of the logarithms are hard to disentangle, and the treatment below seems to be more promising for systematic work.)

To verify that the value of $c(0)$ given by (3.23) and the solution to the

generalised TBA equation is the same as came via the excited solution to the basic TBA, we start by finding the kink form of the generalised TBA system. From (3.7) we have, as $r \rightarrow 0$,

$$\beta_2^{(0)}(r) \sim \log(1/r) - c_2^{(0)}$$

where, for the solution under discussion, $c_2^{(0)}$ is a real constant. Hence

$$\theta_2^{(0)} \sim \log(1/r) - c_2^{(0)} + \frac{\imath\pi}{5}. \quad (3.32)$$

The $\imath\epsilon$ prescription for r means that $\theta_2^{(0)}$ is still (just) inside the strip $0 < \text{Im} \theta_2^{(0)} < \pi/5$. We can take this into account by setting $r = \rho e^{\imath\epsilon}$, with ρ real and ϵ understood to be vanishingly small and positive. The kink form of equations (3.22), (3.26) and (3.23) follows on shifting θ to $\theta + \log(1/\rho)$, defining $\varepsilon_a^{\text{kink}}(\theta) = \varepsilon_a(\theta + \log(1/\rho))$, employing the limiting form of $\theta_2^{(0)}(r)$, and finally taking the $\rho \rightarrow 0$ limit, dropping inessential factors of $\imath\epsilon$:

$$\varepsilon_a^{\text{kink}}(\theta) = \frac{1}{2} m_a r e^\theta + \text{Log}_{\mathcal{C}} S_{a2}(\theta + c^{(0)} - \frac{\imath\pi}{5} + \imath\epsilon) - \sum_{b=1}^2 \phi_{ab} * L_b^{\text{kink}}(\theta); \quad (3.33)$$

$$0 = \frac{1}{2} m_2 e^{-c^{(0)}} e^{\imath\pi/5} + \pi \imath (N_{22} - 1) - \sum_{b=1}^2 \phi_{2b} * L_b^{\text{kink}}(-c^{(0)} + \frac{\imath\pi}{5} - \imath\epsilon); \quad (3.34)$$

$$c(0) = \frac{6}{\pi} \imath m_2 e^{c^{(0)}} e^{\imath\pi/5} + \frac{6}{\pi^2} \sum_{a=1}^2 \int_{-\infty}^{\infty} d\theta \frac{1}{2} m_a e^\theta L_a^{\text{kink}}(\theta). \quad (3.35)$$

(For the last equation, use is also made of the fact that half of the integral contributing to $c(0)$ comes from the left-hand kink system, and half from the right.) Differentiating (3.33) with respect to θ and substituting the resulting expression for $\frac{1}{2} m_a e^\theta$ into (3.35) gives

$$\begin{aligned} c(0) = & \frac{6}{\pi} \imath m_2 e^{c^{(0)}} e^{\imath\pi/5} + \frac{6}{\pi^2} \sum_{a=1}^2 \int_{-\infty}^{\infty} d\theta \left[\frac{\partial}{\partial \theta} \varepsilon_a^{\text{kink}}(\theta) \right. \\ & \left. - \imath \phi_{a2}(\theta + c_2^{(0)} - \frac{\imath\pi}{5}) + \sum_{b=1}^2 \phi'_{ab} * L_b^{\text{kink}}(\theta) \right] L_a^{\text{kink}}(\theta). \end{aligned}$$

The use of (3.34) simplifies this to

$$c(0) = 12(N_{22} - 1) + \frac{6}{\pi^2} \sum_{a=1}^2 \int_{\mathcal{E}_a} \text{Log}_{\mathcal{E}_a}(1 + e^{-\varepsilon}) d\varepsilon$$

$$\begin{aligned}
& + \frac{6}{\pi^2} \sum_{a,b=1}^2 \int_{-\infty}^{\infty} d\theta \left[\phi'_{ab} * L_b^{\text{kink}}(\theta) \right] L_a^{\text{kink}}(\theta) \\
= & 12(N_{22}-1) + \frac{6}{\pi^2} \sum_{a=1}^2 \int_{\mathcal{E}_a} \text{Log}_{\mathcal{E}_a}(1+e^{-\varepsilon}) d\varepsilon \\
& - \frac{3}{\pi^2} \sum_{a,b=1}^2 N_{ab} \left[L_a^{\text{kink}}(\theta) L_b^{\text{kink}}(\theta) \right]_{-\infty}^{\infty} .
\end{aligned}$$

Here \mathcal{E}_a is the contour swept out by $\varepsilon_a^{\text{kink}}$, and $\text{Log}_{\mathcal{E}_a}$ is a continuous choice of the logarithm along this contour. The branch choice made previously implies that $L_b^{\text{kink}}(+\infty) = 0$, while for $L_b^{\text{kink}}(-\infty)$ the $\theta \rightarrow -\infty$ limit of (3.33),

$$\varepsilon_a^{\text{kink}}(-\infty) = 2\pi i N_{a2} + \sum_{b=1}^2 N_{ab} L_b^{\text{kink}}(-\infty), \quad (3.36)$$

can be used. Rearranging and changing variables in the integrals,

$$\begin{aligned}
c(0) & = 12(N_{22}-1) + \frac{6}{\pi^2} \sum_{a=1}^2 \left[L_+(\mathcal{C}_a) - \pi i N_{a2} L_a^{\text{kink}}(-\infty) \right] \\
& = -12 - \frac{6i}{\pi} \varepsilon_2^{\text{kink}}(-\infty) + \frac{6}{\pi^2} \sum_{a=1}^2 L_+(\mathcal{C}_a), \quad (3.37)
\end{aligned}$$

with $L_+(\mathcal{C}_a)$ as defined in (3.9). The contours are a little different from the previous case: a single zero in $z_2(\theta)$ crossed the real axis in the continuation from the basic TBA to the new equation. With no further numerical work we can deduce that this time both contours go below the point $x = -1$. As a result, (3.16) is replaced by

$$\begin{aligned}
\text{Log}_{\mathcal{C}_1}(1+x_1) & = \log|1+x_1| - i\pi; \\
\text{Log}_{\mathcal{C}_2}(1+x_2) & = \log|1+x_2| - i\pi. \quad (3.38)
\end{aligned}$$

The branches of $\text{Log}_{\mathcal{C}_a}(x)$ should be unchanged, and indeed substituting (3.38) into the imaginary part of (3.36) shows that (3.19) still holds. From this point on the evaluation of the integrals runs essentially as before, though note that this time the residue terms do not cancel but rather reinforce each other. The result is

$$\sum_{a=1}^2 L_+(\mathcal{C}_a) = - \sum_{a=1}^2 (\mathcal{L}(1) + \mathcal{L}(1+1/x_a)) + \pi^2 + \frac{i\pi}{2} \log [(1+x_1)(1+x_2)/(x_1 x_2)].$$

Substituting into (3.37), and recalling that $\varepsilon_2^{\text{kink}}(-\infty) = -\text{Log}_{\mathcal{C}_2}(x_2) = -\log(-x_2) + i\pi$, the imaginary parts again cancel and we finally recover $c(0) = -20/7$, just as before. Assuming that the analytic continuations had been performed correctly, this calculation had no option but to give the right answer. We included it anyway to show how the generalised equations can be tackled directly, so long as the branches of the logarithms are handled in a consistent way.

From a numerical point of view, there is a difficulty in the ultraviolet regime. The zeroes in the Y 's at $\pm\beta_2^{(0)}$ entail divergences in the pseudoenergies on the real θ axis, along which the TBA equation is being solved. As a result, direct numerical iteration of the equations, as outlined above, becomes unstable as r approaches the segment $[0, r_c]$ of the real axis. Taking a hint from [4], a useful trick is to remove these divergences explicitly, before proceeding to a solution of the equations. It turns out that this can be done in a particularly nice way. The first step is the following identity, a simple consequence of equation (9) of ref. [12]:

$$\phi_{ad}(\theta) = -\phi_h(\theta) l_{ad}^{[T_2]} + \sum_{b=1}^2 \phi_{ab} * \phi_h(\theta) l_{bd}^{[T_2]} \quad (3.39)$$

where $\phi_h(\theta) = h/(2 \cosh \frac{h\theta}{2})$ and h is here equal to 5. (For a discussion of the T_N -related cases of such identities, see ref. [13].) This can be integrated, using

$$\phi_h(\theta) = \pm i \frac{\partial}{\partial \theta} \text{Log}_{\mathcal{C}} \sigma_h(\theta \pm \frac{i\pi}{h}) \quad , \quad \sigma_h(\theta) = \tanh(\frac{h\theta}{4}) \quad , \quad (3.40)$$

to yield

$$\pm \text{Log}_{\mathcal{C}} S_{ad}(\theta) = \text{Log}_{\mathcal{C}} \sigma_h(\theta \pm \frac{i\pi}{h}) l_{ad}^{[T_2]} - \sum_{b=1}^2 \phi_{ab} * \text{Log}_{\mathcal{C}} \sigma_h(\theta \pm \frac{i\pi}{h}) l_{bd}^{[T_2]} \quad . \quad (3.41)$$

Substituting the $d=2$ case into (3.22), recalling that $\beta_2^{(0)} = \theta_2^{(0)} - i\pi/h$, and absorbing the extra terms by defining

$$\widehat{\varepsilon}_a(\theta) = \varepsilon_a(\theta) - \text{Log}_{\mathcal{C}} \left(\sigma_h(\theta - \beta_2^{(0)}) \sigma_h(\theta + \beta_2^{(0)}) \right) \quad (3.42)$$

and

$$\widehat{L}_a(\theta) = \text{Log}_{\mathcal{C}} \left(\sigma_h(\theta - \beta_2^{(0)}) \sigma_h(\theta + \beta_2^{(0)}) + e^{-\widehat{\varepsilon}_a(\theta)} \right) \quad , \quad (3.43)$$

the excited-state TBA equation has a form identical to the original equation for the ground state:

$$\widehat{\varepsilon}_a(\theta) = m_a r \cosh \theta - \sum_{b=1}^2 \phi_{ab}^* \widehat{L}_b(\theta) . \quad (3.44)$$

The different singularity structure is now entirely encoded in the definitions of $\widehat{\varepsilon}_a$ and \widehat{L}_a , which, in contrast to ε_a and L_a , are not themselves singular at $\pm\beta_2^{(0)}$. The expression for the central charge also has a formal similarity with the original TBA: the integral

$$\frac{1}{2\pi} \int_{-\infty}^{\infty} d\theta e^{\imath k\theta} \log \left(\sigma_h(\theta - x + \imath \frac{\pi}{h}) \sigma_h(\theta + x - \imath \frac{\pi}{h}) \right) = \frac{\imath \sin kx}{k \cosh(\pi k/h)} \quad (3.45)$$

(convergent in the region $|\text{Im } k| < h/2$), taken at $k = \imath$ and $x = \theta_2^{(0)}$, allows equation (3.23) to be rewritten as

$$c(r) = \frac{3}{\pi^2} \sum_{a=1}^2 \int_{-\infty}^{\infty} d\theta m_a r \cosh \theta \widehat{L}_a(\theta) . \quad (3.46)$$

These equations look just the same as the original TBA system. However it is important that they contain an extra parameter, namely the value of $\beta_2^{(0)}$. When handling the system numerically, we can't search for the singularity at $\beta_2^{(0)}$ – it has been explicitly removed – but must instead focus on $\theta_2^{(0)}$, and impose

$$e^{\widehat{\varepsilon}_2(\theta_2^{(0)})} = \imath \coth \left(\frac{5}{2} \theta_2^{(0)} + \frac{\imath\pi}{4} \right) e^{\varepsilon_2(\theta_2^{(0)})} = -\imath \coth \left(\frac{5}{2} \theta_2^{(0)} + \frac{\imath\pi}{4} \right) . \quad (3.47)$$

This method was used to obtain table 1, and also figure 9.

3.4 Type II singular lines

The problems encountered at the end of the last subsection can be traced to the presence of a type II singular line, along which a zero of $Y_a(\theta)$ has vanishing real part. As hinted earlier, the behaviour of the generalised TBA as such a line is crossed has some novel features.

The first point to note is that any initial crossing of the real θ axis by a zero of Y_1 or Y_2 must be preceded by the crossing of a zero of either z_1 or z_2 – this follows from (3.2) and (3.3), and the configuration of the singularities before the continuation begins. Therefore, just prior to the first

crossing of the zero of Y_1 or Y_2 , there will already be an active singularity in the equations, a zero in $z_c(\theta)$, say, at $\theta_c^{(j)}$. Without any significant loss of generality, suppose that this singularity became active as it crossed the real θ axis from below, so that it currently lies in the strip $0 < \text{Im} \theta_c^{(j)} < \pi/5$. The accompanying zero or zeroes of the Y_a , at $\beta_c^{(j)} = \theta_c^{(j)} - i\pi/5$, lie below the real θ axis and at this stage are inactive. The generalised TBA equation for $\varepsilon_a(\theta)$ contains a term

$$\text{Log}_{\mathcal{C}} S_{ac}(\theta - \theta_c^{(j)}) \quad (3.48)$$

which can be traced to the presence of the active singularity at $\theta_c^{(j)}$. There is also an additive contribution to $c(r)$, equal to

$$\frac{6r}{\pi} i m_c \sinh \theta_c^{(j)}. \quad (3.49)$$

Now consider what can happen to these terms as r varies. The simplest option for change is for $\text{Im} \theta_c^{(j)}$ to become once more negative, meaning that a type I singular line has been crossed. Clearly this corresponds to undoing the trapped piece of contour, and the net effect is for the two terms (3.48) and (3.49) to drop out of the equations, returning them to their original state. Note that this change in the generalised TBA equations is signalled by $\beta_c^{(j)}$ leaving the strip $|\text{Im} \beta_c^{(j)}| < \pi/5$.

More subtle is the behaviour when $\text{Im} \theta_c^{(j)}$ grows beyond $\pi/5$, $\beta_c^{(j)}$ crossing the real axis but remaining inside the strip $|\text{Im} \beta| < \pi/5$. This corresponds to the crossing of a type II singular line. (We already discussed a case with $\text{Im} \theta_c^{(j)}$ exactly equal to $\pi/5$, found when r hits the segment $0 < r < r_c$ of the real axis from above. The question currently being addressed would arise if r was then continued beyond this segment into the lower half plane.) As $\text{Im} \theta_c^{(j)}$ passes $\pi/5$, the singularities in the $L_a(\theta)$ at $\beta_c^{(j)}$ cross the real axis. Further terms must be added to the equations, which are conveniently summarised using the incidence matrix of the T_2 diagram, $l_{cb}^{[T_2]}$. The terms (3.48) and (3.49) become

$$\text{Log}_{\mathcal{C}} S_{ac}(\theta - \theta_c^{(j)}) - \sum_{b=1}^2 l_{cb}^{[T_2]} \text{Log}_{\mathcal{C}} S_{ab}(\theta - (\theta_c^{(j)} - i\pi/5)) \quad (3.50)$$

and

$$\frac{6r}{\pi} i m_c \sinh \theta_c^{(j)} - \frac{6r}{\pi} i \sum_{b=1}^2 l_{cb}^{[T_2]} m_b \sinh(\theta_c^{(j)} - i\pi/5) \quad (3.51)$$

respectively. (The minus signs are there because the new singularities are zeroes of $Y_b(\theta)$, rather than $z_c(\theta)$.) The situation seems to have become more complicated, but is helped by the following pair of identities:

$$S_{ac}(\theta - i\pi/5)S_{ac}(\theta + i\pi/5) = \prod_{b=1}^2 S_{ab}(\theta) l_{cb}^{[T_2]} ;$$

$$m_c [\sinh(\theta - i\pi/5) + \sinh(\theta + i\pi/5)] = \sum_{b=1}^2 l_{cb}^{[T_2]} m_b \sinh \theta .$$

Defining $\theta_c^{(j')} = \theta_c^{(j)} - 2i\pi/5$, the terms (3.50) and (3.51) simplify to

$$- \text{Log}_c S_{ac}(\theta - \theta_c^{(j')}) \tag{3.52}$$

and

$$- \frac{6r}{\pi} i m_c \sinh \theta_c^{(j')} . \tag{3.53}$$

These are exactly the extra terms that would have been found had a singularity in $L_c(\theta)$, a zero of $z_c(\theta)$, crossed the real θ axis, though from above rather than from below. From (3.2) or (3.3), there is indeed a zero of $z_c(\theta)$ at $\theta_c^{(j')}$, so this reinterpretation of the equation is consistent with the singularity pattern actually found.

It is worth pausing to consider what has happened. The situation under discussion was the crossing of a type II singular line, and we have shown that it does not lead to a fundamentally different equation, but just a relocation of an already-active singularity, back into the strip $|\text{Im} \theta| < \pi/5$. This is in contrast to the crossing of a type I singular line, which always either adds or subtracts a singularity from the active list. It can now be deduced that any equation obtained from the ground-state TBA system by analytic continuation in r can be rewritten in such a way that the only active singularities correspond to zeroes of z_1 or z_2 in the strip $|\text{Im} \theta| < \pi/5$. Furthermore, in the rewritten equations a zero of $z_c(\theta)$ in this strip will be active if and only if $\beta_c^{(j)}$, the position of the accompanying zero of $Y_1(\theta)$ and/or $Y_2(\theta)$, satisfies $|\text{Im} \beta_c^{(j)}| < \pi/5$. This observation provides the bridge between our approach and the methods advocated in refs. [17, 4].

Finally, we should examine the behaviour of the equations for the first excited state near to $r=r_c$. Recall that in the far infrared, $\theta_2^{(0)}(r)$ approached $i\pi/10$ from above. As r decreases, $\theta_2^{(0)}$ grows and finally, at $r=r_c$,

it arrives at $i\pi/5$. This is necessary for there to be a continuous transition to the singularity pattern observed when r is less than r_c . There are also inactive singularities associated with zeroes of Y_1 and Y_2 , located at $\pm\beta_2^{(0)} = \pm(\theta_2^{(0)} - i\pi/5)$, and as r approaches r_c , these singularities start to pinch the real axis. This poses a mild puzzle, the exact converse of that discussed in section 3.2: there, a branch point of $c(r)$ was present and yet there was no evidence of an integration contour being pinched, while here, contours are being pinched and yet (because r is real) we do not expect there to be a branch point. The absence of this branch point can be understood if we use the standard technique for analysing a pinch singularity, as described, for example, in chapter 2 of [19]. This involves continuing r in a complete circle around the potentially singular point, and then comparing the result with the uncontinued situation in order to find the discontinuity over the putative branch cut.

Near to r_c , we found the following dependence of $\theta_2^{(0)}$ on r :

$$\theta_2^{(0)}(r) = i\frac{\pi}{5} + B(r_c - r)^{1/2} + O(r_0 - r) \quad (3.54)$$

with $B = 0.3763188677(2)$. This gives a good control over the positions of the singularities, allowing their changing status to be followed as r traces out a small circle about r_c . At first sight the situation after continuation looks very different from that before: the active singularities at $\pm\theta_2^{(0)}$ have left the strip $|\text{Im } \theta| < \pi/5$, their former positions now being occupied by a pair of inactive singularities, whilst the two singularities at $\pm\beta_2^{(0)}$ have swapped over and become active. However, while the assignments of singularities as active or inactive have changed, their overall pattern has not. Even better, a moment's thought shows that what has happened is just as would be expected, given that the type II singular line running from 0 to r_c along the real axis was crossed exactly once during the continuation. The earlier discussion of such situations applies, and if the equations are rewritten as described above, they return to exactly the form that they had before the continuation was performed. Hence the discontinuity is zero, and there is no branch cut after all. The functions $Y_a(r, \theta)$ are single-valued in the neighbourhood of $r=r_c$, despite the square root in (3.54), which merely shows that the labelling of the singularities is not single-valued as r_c is encircled – it does not of itself require that the Y 's should be multiple-valued.

One particular consequence of this discussion is that the type II singular line actually terminates at $r=r_c$. This behaviour is special to the lines

associated with zeroes of the Y 's, and is possible because the number of zeroes of the $Y_a(\theta)$ in the strip $|\text{Im } \theta| < \pi/5$ does not change as such lines are crossed. By contrast, type I lines separate regions of validity of fundamentally different TBA equations, and so they cannot just stop at isolated values of r . In fact, they always seem to be anchored on some covering point of $r=0$, although we cannot absolutely rule out other closed loops elsewhere on the Riemann surface.

3.5 On to the third sheet

The third sheet can be reached by analytic continuation around either B or \tilde{B} on figure 1. The point \tilde{B} lies in a part of the Riemann surface described by the basic TBA equations (2.3) and (2.4), and continuing around \tilde{B} in an anticlockwise sense we find a third set of solutions to this system. If r is now returned to the origin keeping $\arg(r)$ greater than approximately $2.11\pi/5$, no singularities cross the real θ axis and a new kink solution to the basic TBA is uncovered. The value of $c(0)$ on the third sheet can now be calculated much as before, using the new forms of the contours \mathcal{C}_1 and \mathcal{C}_2 as the necessary input into the formula (3.8). We found that \mathcal{C}_1 runs from the origin to a positive real endpoint x_1 , with no winding about $x = -1$, and that \mathcal{C}_2 runs from the origin to a point $x_2 < -1$, passing above $x = -1$. The relevant stationary solution to the Y -system is therefore the $s=5$ case of (3.11):

$$x_1 = 1/y_1^{(5)} \quad , \quad x_2 = 1/y_2^{(5)} \quad .$$

From the contours follow the relevant branches of the logarithms: first we deduce

$$\begin{aligned} \text{Log}_{\mathcal{C}_1}(1+x_1) &= \log|1+x_1|; \\ \text{Log}_{\mathcal{C}_2}(1+x_2) &= \log|1+x_2| + i\pi, \end{aligned} \quad (3.55)$$

and then feeding this into the imaginary part of (3.17) establishes that

$$\begin{aligned} \text{Log}_{\mathcal{C}_1}(x_1) &= \log|x_1| - 2i\pi; \\ \text{Log}_{\mathcal{C}_2}(x_2) &= \log|x_2| - 3i\pi. \end{aligned} \quad (3.56)$$

The branch of $\text{Log}_{\mathcal{C}_1}(x_1)$ means that, despite x_1 being a positive real number, $L_+(\mathcal{C}_1)$ has an imaginary part. Extracting this and dealing with the rest via the change of variables $t = x/(1+x)$,

$$L_+(\mathcal{C}_1) = \mathcal{L}(x_1/(1+x_1)) + i\pi \log(1+x_1) \quad .$$

For $L_+(\mathcal{C}_2)$ the calculation is just as described in section 3.1, modulo the revised branch of $\text{Log}_{\mathcal{C}_2}(x)$. The result is

$$L_+(\mathcal{C}_2) = -\mathcal{L}(1) - \mathcal{L}(1 + 1/x_2) - \frac{3}{2}\pi^2 + \frac{1}{2}i\pi \log [x_2(1+x_2)^3] .$$

Adding the two together, the stationary Y-system can be used to show that the imaginary part of the total vanishes, and via the sum rule (3.15) we obtain

$$c(0) = -68/7$$

which is indeed the expected answer for the third sheet, given that at $r=0$ it sees the state generated by φ_{11} .

During the continuation around \tilde{B} , the singularity at $\beta_2^{(0)}$ remains in the left-hand kink system, but those at $\beta_1^{(0)}$ and $\beta_2^{(1)}$ defect to the right-hand system. In the notation of (3.7), the amounts to

$$\begin{aligned} \nu_1^{(0)} &= -1, & \nu_2^{(0)} &= +1, \\ \nu_1^{(j>0)} &= +1, & \nu_2^{(1)} &= -1, \\ & & \nu_2^{(j>1)} &= +1. \end{aligned} \tag{3.57}$$

Although the singularity at $\beta_2^{(0)}$ doesn't change its allegiance, it does move in a significant way, and in the new kink limit it comes to be symmetrically placed with the defecting $-\beta_2^{(1)}$. The relevant data about the asymptotic disposition of singularities is conveniently summarised using the constants $c_a^{(j)}$ defined by (3.7):

$$\begin{aligned} \text{Im } c_1^{(0)} &= 0, & \text{Im } c_2^{(0)} &= +1.10933(9)\frac{\pi}{5}, \\ \text{Im } c_1^{(j>0)} &= \pm\frac{7\pi}{10}, & \text{Im } c_2^{(1)} &= -1.10933(9)\frac{\pi}{5}, \\ & & \text{Im } c_2^{(j>1)} &= \pm\frac{7\pi}{10}. \end{aligned} \tag{3.58}$$

In addition

$$\text{Re } c_2^{(0)} = \text{Re } c_2^{(1)}. \tag{3.59}$$

The imaginary parts of the singularity positions are important because, via equations (3.20) and (3.21), they determine the directions along which singular lines leave the point $r=0$ on the Riemann surface. The pattern here on the third sheet is much richer than previously seen: in the sector

$\pi/2 > \arg(r) \geq 0$, there are three type I lines and two type II lines. Their directions are:

$$\arg(r) = 2.10933(9)\frac{\pi}{5} \quad (\text{for } z_2(\theta)); \quad (3.60)$$

$$\arg(r) = 1.10933(9)\frac{\pi}{5} \quad (\text{for } Y_2(\theta)); \quad (3.61)$$

$$\arg(r) = \frac{\pi}{5} \quad (\text{for } z_1(\theta)); \quad (3.62)$$

$$\arg(r) = 0.10933(9)\frac{\pi}{5} \quad (\text{for } z_2(\theta)); \quad (3.63)$$

$$\arg(r) = 0 \quad (\text{for } Y_1(\theta)). \quad (3.64)$$

(Just beyond this sector there is, as always, an infinite accumulation of type I lines, with $\arg(r) = 7\pi/10 - \pi/5 = \pi/2$.) As r moves towards the real axis keeping near to the origin, with $\arg(r)$ decreasing from just below $\pi/2$ to zero, the singular lines are crossed in turn, and various generalised TBA equations are encountered. First, the basic TBA applies; then, as the type I line (3.60) is passed, $\beta_2^{(1)}$ enters the strip $|\text{Im } \beta| < \pi/5$. The zeroes of $z_2(\theta)$ at $\pm\theta_2^{(1)}$ cross the real θ axis and we move into territory described by equations (3.22), (3.23) and (3.26). However this time it is the singularities at $\pm\theta_2^{(1)}$ that have become active, rather than those at $\pm\theta_2^{(0)}$, and so strictly speaking the labelling in the generalised TBA equations should be adjusted accordingly. This has an interesting consequence. The same region of the Riemann surface, namely that part of the third sheet described by equations (3.22), (3.23) and (3.26), can alternatively be reached from the basic TBA by first continuing around the point A , and then looping anticlockwise around the point B . As A is encircled, the singularities at $\pm\theta_2^{(0)}$ become active, and these remain the only active singularities during the rest of the continuation. Their ultimate positions are those at which the singularities at $\pm\theta_2^{(1)}$ had previously been found, when the continuation had been about \tilde{B} . Therefore, if the first continuation is combined with the reverse of the second, the net effect is to swap over $\theta_2^{(0)}$ and $\theta_2^{(1)}$. In the last subsection it was observed that a singularity can be swapped with its negative under continuation around certain points on the Riemann surface; here is an example of a more complicated exchange, associated with a continuation around a non-trivial cycle on the surface.

Passing the type II line (3.61), the next singularities, zeroes of $Y_2(\theta)$ at $\pm\beta_2^{(1)}$, cross the real axis. This does not change the set of $\beta_a^{(j)}$ inside the strip $|\text{Im } \beta| < \pi/5$, and the only effect of the transition is to reallocate the

active singularities. Equations (3.22), (3.23) and (3.26) continue to hold, but now with the active singularities at $\pm\theta_2^{(1')}(r) = \pm(\theta_2^{(1)}(r) - 2\pi/5)$.

A genuinely new equation is only found when the type I line (3.62) is crossed. The singularities in $L_1(\theta)$ at $\pm\theta_1^{(0)}$ become active, and a generalised TBA equation involving four active singularities results. It should by now be clear that the labelling of singularities is path-dependent, and so for notational simplicity we shall opt to label the two pairs of active singularities as $\pm\theta_1^{(0)}$ and $\pm\theta_2^{(0)}$, with $\theta_1^{(0)}$ and $\theta_2^{(0)}$ both having positive imaginary parts. This means that $\theta_1^{(0)}$ belongs to the right-hand kink system, and $\theta_2^{(0)}$ to the left-hand one. The new equation is then

$$\varepsilon_a(\theta) = m_a r \cosh \theta + \text{Log}_{\mathcal{C}} \frac{S_{a1}(\theta - \theta_1^{(0)}) S_{a2}(\theta - \theta_2^{(0)})}{S_{a1}(\theta + \theta_1^{(0)}) S_{a2}(\theta + \theta_2^{(0)})} - \sum_{b=1}^2 \phi_{ab} * L_b(\theta) . \quad (3.65)$$

with

$$c(r) = \frac{12r}{\pi} i (m_1 \sinh \theta_1^{(0)} + m_2 \sinh \theta_2^{(0)}) + \frac{3}{\pi^2} \sum_{a=1}^2 \int_{-\infty}^{\infty} d\theta m_a r \cosh \theta L_a(\theta) . \quad (3.66)$$

There are now two independent singularity positions to be fixed, and the equations for these are found by setting θ equal to $\theta_1^{(0)}$ and then $\theta_2^{(0)}$ in (3.65). This gives

$$i\pi = m_a r \cosh \theta_a^{(0)} + \sum_{b=1}^2 \text{Log}_{\mathcal{C}} \frac{S_{ab}(\theta_a^{(0)} - \theta_b^{(0)})}{S_{ab}(\theta_a^{(0)} + \theta_b^{(0)})} - \sum_{b=1}^2 \phi_{ab} * L_b(\theta_a^{(0)}) , \quad a = 1, 2 . \quad (3.67)$$

There are $2n\pi i$ ambiguities on the left-hand sides of these equations, both from the branch choices involved in solving $\exp(-\varepsilon_a(\theta_a^{(0)})) = -1$, and from the memory of the particular path of continuation implicit in the notation $\text{Log}_{\mathcal{C}}$. As seen in the last subsection, it is important to sort these out if a direct analytic treatment of the ultraviolet asymptotics is to be given. We will leave further discussion of this point for now, contenting ourselves with the calculation that was performed earlier, in the sector of the third sheet where the zero-singularity TBA applied. These worries are unimportant for numerical work, and using the exponentiation and inversion idea described earlier, equations (3.65) – (3.67) can be solved over large regions of the complex r plane. In particular, they turn out to hold even when r is real, so long as the infrared regime has been reached. However near to $r=0$

there is one more transition to go, caused by the type I line (3.63). As this singular line is passed, the zero of $Y_2(\theta)$ at $\beta_2^{(0)}$ leaves the strip $|\text{Im } \beta| < \pi/5$ and the associated singularity ceases to be active. There is now only one pair of active singularities, and in contrast to the previous example, these singularities are in L_1 and not L_2 . The relevant equations can be found from (3.65) – (3.67) by deleting all terms involving $\theta_2^{(0)}$:

$$\varepsilon_a(\theta) = m_a r \cosh \theta + \text{Log}_{\mathcal{C}} \frac{S_{a1}(\theta - \theta_1^{(0)})}{S_{a1}(\theta + \theta_1^{(0)})} - \sum_{b=1}^2 \phi_{ab} * L_b(\theta) , \quad (3.68)$$

$$c(r) = \frac{12r}{\pi} i \sinh \theta_1^{(0)} + \frac{3}{\pi^2} \sum_{a=1}^2 \int_{-\infty}^{\infty} d\theta m_a r \cosh \theta L_a(\theta) , \quad (3.69)$$

and

$$i\pi = m_1 r \cosh \theta_1^{(0)} + \text{Log}_{\mathcal{C}} \frac{S_{11}(0)}{S_{11}(2\theta_1^{(0)})} - \sum_{b=1}^2 \phi_{ab} * L_b(\theta_a^{(0)}) . \quad (3.70)$$

These equations should hold in the sector $0.10933(9)\pi/5 > \arg(r) > 0$ while $|r|$ remains small enough that the splitting of the pseudoenergies into left and right kink systems holds. However the proximity of the type II singular line (3.64), and the resulting presence of zeroes of $Y_1(\theta)$ near to the real θ axis, means that a direct numerical treatment fails, at least with the methods that we have at present. Fortunately the equations can be recast into a more tractable form. As before, the key is to use the identity (3.41) to eliminate some of the singular behaviour in ε_a and L_a . Here, the $d=1$ case of (3.41) is relevant, and the revised definitions of ε_a and L_a are

$$\widehat{\varepsilon}_a(\theta) = \varepsilon_a(\theta) - l_{a1}^{[T_2]} \text{Log}_{\mathcal{C}} \left(\sigma_h(\theta - \beta_1^{(0)}) \sigma_h(\theta + \beta_1^{(0)}) \right) \quad (3.71)$$

and

$$\widehat{L}_a(\theta) = \text{Log}_{\mathcal{C}} \left(\left(\sigma_h(\theta - \beta_1^{(0)}) \sigma_h(\theta + \beta_1^{(0)}) \right)^{l_{a1}^{[T_2]}} + e^{-\widehat{\varepsilon}_a(\theta)} \right) . \quad (3.72)$$

Only ε_2 and L_2 are changed by this manoeuvre, as expected given (3.3). The generalised TBA then falls into the more traditional form of equations (3.44) and (3.46), with of course the proviso that the singularities must be correctly placed. This equation turns out to be valid for real r out to $r = r_{c_2} \approx 4.7271(0)$; some numerical results are compared with TCSA data in table 3 of appendix B.

To understand why the equation breaks down at $r = r_{c_2}$, we tracked the motion of the first few singularities as r varied on the segment $[0, r_{c_2}]$. At $r = 0$, their positions follow from the kink system. Labelling the singularities consistently with (3.65), the right-hand kink system contains amongst other things an active singularity at $\theta_1^{(0)}$, with imaginary part equal to $i\pi/5$, and a pair of conjugately-placed inactive singularities at $-\theta_2^{(0)}$ and $\theta_2^{(1)}$, with imaginary parts equal to $0.10933(9)\pi/5$ and $-0.10933(9)\pi/5$ respectively. As r increases, the real part of $-\theta_2^{(0)}$ decreases, until at $r = r_{c_1} = 4.691(0)$ it vanishes completely and the singularity at $-\theta_2^{(0)}$, part of the right-hand kink system, collides with one at $-\theta_2^{(1)}$, coming in from the left-hand system. At this stage the imaginary parts of these singularities are still positive. During the collision, the singularities undergo a 90 degree ‘scattering’ and for r just larger than r_{c_1} , they have turned into a pair of singularities on the positive imaginary axis, one heading up, and one heading down towards $\theta=0$. Choosing to allocate the label $-\theta_2^{(0)}$ to the second of these, we were able to track its progress down the imaginary θ axis for a short way before our numerical methods became unstable. Extrapolating beyond this point and also making use of data from larger values of r , we found that $-\theta_2^{(0)}$ hits the origin when r arrives at r_{c_2} . The natural explanation for this behaviour is that the type I line (3.63), which started at the origin moving away from the real r axis, has curved round and hit the real axis again. (It then returns to the origin on the complex-conjugated path in the lower half plane.) We confirmed this picture by tracking singularity positions for complex values of r , and conclude that the domain of applicability of equations (3.68) – (3.70) is restricted to a small neighbourhood of the segment $[0, r_{c_2}]$ of the real axis. As this region is left, the singularities at $\pm\theta_2^{(0)}$ cross the real θ axis and the more complicated equations (3.65) – (3.70) come into operation. The singularity movement described so far is plotted as the lines labelled $\text{Re}(-\theta_2^{(0)})$ and $\text{Im}(-\theta_2^{(0)})$ on figure 10, showing first the vanishing of the real part at r_{c_1} , and then the crossing of $-\theta_2^{(0)}$ into the lower half plane at r_{c_2} . Looking elsewhere on the figure, we see that $\text{Im}\theta_1^{(0)}$ remains equal to $\pi/5$ as the point r_{c_2} is passed. This means that the singularities at $\pm\beta_1^{(0)}$ are still on the real θ axis, and the transition to the infrared regime is not quite complete. For numerical work, we must continue to use the modified definitions (3.71) and (3.72) to cope with these singularities. Whilst it is only the singularities at $\pm\beta_1^{(0)}$ that have to be dealt with in this way, there are now also active singularities at $\pm\theta_2^{(0)}$, and the equations are more elegant

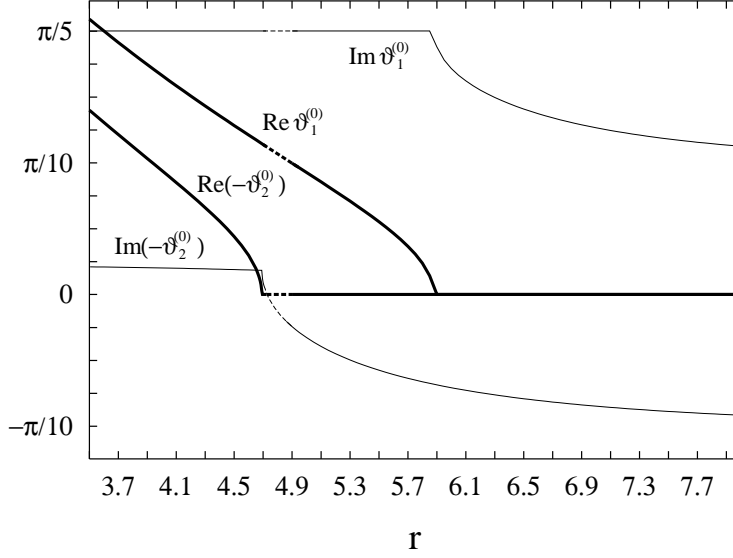


Figure 10: Singularity movement for the second one-particle state: the dotted segments indicate the region where the numerics failed to converge, and were obtained by extrapolation from larger values of r . Transitions are at $r_{c_1} = 4.691(0)$, $r_{c_2} = 4.7271(0)$, and $r_{c_3} = 5.8786(1)$.

if the associated points $\pm\beta_2^{(0)}$ are ‘desingularised’ at the same time: setting

$$\widehat{\varepsilon}_a(\theta) = \varepsilon_a(\theta) - \text{Log}_C \prod_{d=1}^2 \left(\sigma(\theta - \beta_d^{(0)}) \sigma(\theta + \beta_d^{(0)}) \right)_{ad}^{[T_2]} \quad (3.73)$$

and

$$\widehat{L}_a(\theta) = \text{Log}_C \left(\prod_{d=1}^2 \left(\sigma(\theta - \beta_d^{(0)}) \sigma(\theta + \beta_d^{(0)}) \right)_{ad}^{[T_2]} + e^{-\widehat{\varepsilon}_a(\theta)} \right), \quad (3.74)$$

they again acquire the form of equations (3.44) and (3.46). This time, though, there are two independent singularity positions to fix:

$$\begin{aligned} e^{\widehat{\varepsilon}_1(\theta_1^{(0)})} &= -i \coth \left(\frac{5}{2} \theta_1^{(0)} + \frac{i\pi}{4} \right); \\ e^{\widehat{\varepsilon}_2(\theta_2^{(0)})} &= -i \coth \left(\frac{5}{2} \theta_2^{(0)} + \frac{i\pi}{4} \right). \end{aligned} \quad (3.75)$$

These equations were used to obtain tables 4 and 5 of appendix B; the second set was also confirmed by the direct use of the system (3.65) – (3.67). As can be seen from figure 10, there is a final transition to the infrared regime, at $r = r_{c_3} \approx 5.8786(1)$, where the real part of $\theta_1^{(0)}$ vanishes and all active singularities take up positions on the imaginary axis.

As r grows further, both $\theta_1^{(0)}$ and $\theta_2^{(0)}$ approach $\imath\pi/10$, and the identity

$$m_2 = 2 \sin\left(\frac{\pi}{10}\right)(m_1 + m_2) \quad (3.76)$$

leads to the result $c(r) \sim -6m_2r/\pi$, or $E(\lambda, R) \sim E_{\text{bulk}}(\lambda, R) + M_2$. This is as expected, and just as before we can supplement the result by calculating two further corrections. For $a = 1, 2$ we set $\theta_a^{(0)}(r) = \imath\pi/10 + \delta_a(r)$, where both $\delta_1(r)$ and $\delta_2(r)$ are purely imaginary for real r larger than r_{c_3} , and tend to zero as $r \rightarrow \infty$. Imposing (3.67), with the convolution terms ignored as being subleading, leads to the following pair of conditions:

$$\begin{aligned} \frac{S_{12}(\delta_1 - \delta_2)}{S_{11}(\imath\pi/5 + 2\delta_1)S_{12}(\imath\pi/5 + \delta_1 + \delta_2)} &\sim e^{-m_1 r \cos(\pi/10)} ; \\ \frac{S_{12}(\delta_2 - \delta_1)}{S_{12}(\imath\pi/5 + \delta_1 + \delta_2)S_{22}(\imath\pi/5 + 2\delta_2)} &\sim e^{-m_2 r \cos(\pi/10)} . \end{aligned}$$

(Note that with the equations exponentiated in this way the branch ambiguities have gone.) It will be convenient to have a notation for the most singular parts of the various poles controlling these equations: given a function $f(\theta)$, we let $\mathcal{R}f(\theta_0)$ denote the leading coefficient of its Laurent expansion about θ_0 :

$$f(\theta) = \mathcal{R}f(\theta_0)(\theta - \theta_0)^p + \sum_{k=p+1}^{\infty} A_k(\theta - \theta_0)^k ; \quad \mathcal{R}f(\theta_0) \neq 0. \quad (3.77)$$

(If the pole at θ_0 is simple, then $\mathcal{R}f(\theta_0)$ is just the residue.) The limiting behaviour of δ_1 and δ_2 is then determined by

$$\begin{aligned} \frac{1}{S_{11}(\imath\pi/5)} \frac{\delta_1 + \delta_2}{\mathcal{R}S_{12}(\imath\pi/5)} &\sim e^{-m_1 r \cos(\pi/10)} ; \\ \frac{\delta_1 + \delta_2}{\mathcal{R}S_{12}(\imath\pi/5)} \frac{2\delta_2}{\mathcal{R}S_{22}(\imath\pi/5)} &\sim e^{-m_2 r \cos(\pi/10)} . \end{aligned}$$

Solving, and using (2.1) for the S-matrix elements, we have

$$\begin{aligned} \delta_2(r) &\sim -\imath \tan\left(\frac{2\pi}{5}\right) e^{-(m_2 - m_1)r \cos(\pi/10)}, \\ \delta_1(r) &\sim 2\imath \tan\left(\frac{3\pi}{10}\right) \tan\left(\frac{2\pi}{5}\right)^2 e^{-m_1 r \cos(\pi/10)} - \delta_2(r). \end{aligned}$$

Note that $i\pi/10$ is approached from above by $\theta^{(0)}$, and from below by $\theta_2^{(0)}$. The leading effect that this has on the value of $c(r)$ is through the term $\frac{12r}{\pi}i(m_1 \sinh \theta_1^{(0)} + m_2 \sinh \theta_2^{(0)})$ in (3.66). The result matches the contributions of the field-theoretic μ -terms, given in appendix A. Notice that this time there are two distinct exponentials, reflecting the two processes $2 \rightarrow 12 \rightarrow 2$ and $2 \rightarrow 11 \rightarrow 2$. A different type of correction comes from the thus-far neglected integral in (3.66), using the first two terms on the right-hand side of (3.65) to estimate $L_a(\theta)$. The modifications to $\theta_1^{(0)}$ and $\theta_2^{(0)}$ have a subleading effect on this term, and so their asymptotic values of $i\pi/10$ can be used, whereupon the following identity becomes relevant:

$$\frac{S_{a1}(\theta + \frac{i\pi}{10}) S_{a2}(\theta + \frac{i\pi}{10})}{S_{a1}(\theta - \frac{i\pi}{10}) S_{a2}(\theta - \frac{i\pi}{10})} = S_{a2}(\theta + \frac{i\pi}{2}). \quad (3.78)$$

The final result is

$$c(r) \sim \frac{-6r}{\pi} \left(m_2 + 2C_1 m_1 e^{-m_1 r \sin(2\pi/5)} + C_2 m_1 e^{-m_1 r \sin(\pi/5)} - \frac{1}{2\pi} \sum_{a=1}^2 \int_{-\infty}^{\infty} d\theta m_a \cosh \theta S_{2a}(\theta + \frac{i\pi}{2}) e^{-r m_a \cosh \theta} \right). \quad (3.79)$$

where

$$C_1 = 2 \cos\left(\frac{\pi}{10}\right) \tan\left(\frac{3\pi}{10}\right) \tan\left(\frac{2\pi}{5}\right)^2 = 24.79837\dots \quad (3.80)$$

and

$$C_2 = -2 \sin\left(\frac{\pi}{5}\right) \tan\left(\frac{2\pi}{5}\right) = -3.61803\dots \quad (3.81)$$

and the identity

$$(m_2 - m_1) \cos(\pi/10) = m_1 \sin(\pi/5) \quad (3.82)$$

was used to rewrite the second μ -term. These match the predictions from field theory recorded in table 2 of [18], or appendix A.

4 Generalisations

In this section we indicate how some of the above results for the T_2 model can be extended to the rest of the T_N series. Most of our analysis is confined to the infrared region, where an elegant pattern emerges. Even for real r , the story becomes more complicated outside this region, as the movement

of singularities causes the equations to change their forms. The simplest examples were seen in refs. [4, 5] and also in section 3.3 above, with the single transition that could be traced to the arrival of a pair of singularities exactly on the real θ axis. As was seen in that section, the effect is rather mild – in particular, the infrared equations continue to apply if r is given an infinitesimal imaginary part. The case studied in section 3.5, the second 1-particle state of the T_2 theory, provides the first example of the more complicated behaviour that we expect to see in the general case: one pair of active singularities, present in the infrared, disappears completely in the ultraviolet. For general N we will see that the inverse process is also possible: a certain number of new singularities can become active at small r . This will be described at the end of the section, using an example from the T_4 theory.

Our initial conjecture is based on the behaviour already observed for $N=1$ and $N=2$, and the following two identities. If we set

$$B = N - A + 1$$

then

$$2 \sin \frac{\pi}{2h} \sum_{b=B}^N m_b = m_A \quad (4.1)$$

and

$$\prod_{b=B}^N \frac{S_{ab}(\theta + i\frac{\pi}{2h})}{S_{ab}(\theta - i\frac{\pi}{2h})} = S_{Aa}(\theta + i\frac{\pi}{2}) \quad (4.2)$$

These generalise equations (3.28),(3.30) and (3.76),(3.78) respectively, and make natural the supposition that when r is sufficiently large, the A^{th} one-particle state is exactly described by a generalised TBA equation with A pairs of active singularities, these singularities being found in the pseudoenergies $\varepsilon_b(\theta)$, $b = B \dots N$, with all of them tending to $i\pi/2h$ in the infrared limit. Assuming that this singularity pattern can be achieved through some path of continuation from the ground state, the generalised TBA equation must then be

$$\varepsilon_a(\theta) = m_a r \cosh \theta + \sum_{b=B}^N \text{Log}_c \frac{S_{ab}(\theta - \theta_b^{(0)})}{S_{ab}(\theta + \theta_b^{(0)})} - \sum_{b=1}^N \phi_{ab} * L_b(\theta) , \quad (4.3)$$

with the active singularity positions $\theta_a^{(0)}$, $a = B \dots N$, determined by the

equations

$$i\pi = m_a r \cosh \theta_a^{(0)} + \sum_{b=B}^N \text{Log}_{\mathcal{C}} \frac{S_{ab}(\theta_a^{(0)} - \theta_b^{(0)})}{S_{ab}(\theta_a^{(0)} + \theta_b^{(0)})} - \sum_{b=1}^N \phi_{ab} * L_b(\theta_a^{(0)}) , \quad (4.4)$$

and $c(r)$ given by the formula

$$c(r) = \frac{12r}{\pi} i \left(\sum_{b=B}^N m_b \sinh \theta_b^{(0)} \right) + \frac{3}{\pi^2} \sum_{a=1}^N \int_{-\infty}^{\infty} d\theta m_a r \cosh \theta L_a(\theta) . \quad (4.5)$$

At large r the dominant term is found by setting $\theta_a^{(0)} = i\pi/2h$ and using (4.1), giving $c(r) \sim -6m_A r/\pi$ or $E(\lambda, R) \sim E_{\text{bulk}}(\lambda, R) + M_A$. This is correct for a one-particle state with mass m_A . A couple of further corrections can be obtained exactly. The simplest to find is the F -term, and this comes on using the asymptotic $\varepsilon_a(\theta) \sim m_a r \cosh \theta - \text{Log}_{\mathcal{C}} S_{aA}(\theta + i\pi/2)$ in (4.5) (equation (4.2) having been used in order to simplify the ratio of S-matrices appearing in (4.3)). This gives the following correction to $c(\infty)$:

$$\frac{3r}{\pi^2} \sum_{b=1}^N \int_{-\infty}^{\infty} d\theta m_b \cosh \theta S_{Ab}(\theta + \frac{i\pi}{2}) e^{-m_b r \cosh \theta} . \quad (4.6)$$

With the leading asymptotic of the ground state subtracted off, this matches the F -term (A.1). The derivation of the second correction is more tedious. We set $\theta_a^{(0)} = i\pi/2h + \delta_a$, with δ_a purely imaginary, and start from an infrared form of equation (4.4), obtained by dropping the convolution term and then exponentiating:

$$\prod_{b=B}^N \frac{S_{ab}(\delta_a - \delta_b)}{S_{ab}(i\pi/h + \delta_a + \delta_b)} \sim -e^{-r m_a \cosh \theta_a^{(0)}} , \quad a = B, B+1, \dots N . \quad (4.7)$$

A simple consideration of the signs of the terms in these equations, using

$$\text{Sign } S_{ab}(ix) = \begin{cases} (-1)^{\delta_{ab}} & -\pi/h < x < \pi/h \\ (-1)^{\delta_{ab} + l_{ab}^{[TN]}} & \pi/h < x < 2\pi/h \end{cases}$$

for x real, and the explicit form of $l_{ab}^{[TN]}$, establishes that

$$\text{Sign } \frac{\delta_a}{i} = (-1)^{B+a} , \quad a = B, B+1, \dots N ,$$

These values will modify $c(r)$, at leading order, through a correction term equal to

$$\begin{aligned}
\Delta_\mu c(r) &= \frac{12r}{\pi} \imath \sum_{b=B}^N m_b \cos(\pi/2h) \delta_b \\
&= \frac{12r}{\pi} \imath \left[\sum_{b=B}^{N-1} \mu_b (\delta_b + \delta_{b+1}) + \mu_N \delta_N \right] \\
&= \frac{6r}{\pi} \imath \left[\sum_{b=B}^{N-1} 2\mu_b K_b e^{-\mu_b r} + \mu_N K_N e^{-\mu_N r} \right]. \tag{4.8}
\end{aligned}$$

The calculation now splits into two. First, consider a term in the final sum for which $b-B$ is odd, equal to $2k-1$. Then we can use the following mass relation:

$$\cos(\pi/2h) \sum_{c=B}^{B+2k-1} (-1)^{B+c+1} m_c = m_k \sin\left(\frac{A-k}{h}\pi\right),$$

or

$$\mu_{B+2k-1} = \mu_{A,k,A-k},$$

where the notation $\mu_{A,k,A-k}$ is as used in equations (A.2) and (A.5). Recalling that $\Delta E(R) = -\frac{\pi}{6R} \Delta c(r) = -\frac{M_1 \pi}{6r} \Delta c(r)$ and comparing with the formulae of appendix A, we see that the correction due to the α -process $A \rightarrow k, A-k \rightarrow A$ will be reproduced, so long as the following identity between S-matrix residues holds:

$$-\mathcal{R} \left(\prod_{c=B}^{B+2k-1} \left(S_{Ac} \left(\imath \frac{h+1}{2h} \pi \right) \right)^{(-1)^{B+c+1}} \right) = \mathcal{R} S_{Ak} \left(\imath \frac{A-k}{h} \pi \right).$$

We checked this algebraically up to $N=5$, and then numerically to $N=15$. Up to a sign ambiguity encountered when taking a square root, the identity can also be deduced from the following curious property of the S-matrix elements:

$$\prod_{c=B}^{B+2k-1} \left(S_{Ac}(\theta + \imath \frac{h+1}{2h} \pi) S_{Ac}(\theta + \imath \frac{h-1}{2h} \pi) \right)^{(-1)^{B+c+1}} = \frac{S_{Ak}(\theta + \imath \frac{A-k}{h} \pi)}{S_{Ak}(\theta - \imath \frac{A-k}{h} \pi)}.$$

If $b-B = 2k$ is even, the story is much the same. The relevant mass relation is

$$\cos(\pi/2h) \sum_{c=B}^{B+2k} (-1)^{B+c} m_c = m_{N-k} \sin\left(\frac{A+N-k}{h}\pi\right),$$

or

$$\mu_{B+2k} = \mu_{A, N-k, N+1-A+k}.$$

This has a chance to match the β correction (A.6), from the process $A \rightarrow N-k, N+1-A+k \rightarrow A$. The necessary residue identity is

$$\mathcal{R} \left(\prod_{c=B}^{B+2k} \left(S_{Ac} \left(\imath \frac{h+1}{2h} \pi \right) \right)^{(-1)^{B+c}} \right) = \mathcal{R} S_{A, N-k} \left(\imath \frac{A+N-k}{h} \pi \right),$$

which follows, again up to a sign, from another property of the S-matrix elements:

$$\prod_{c=B}^{B+2k} \left(S_{Ac} \left(\theta + \imath \frac{h+1}{2h} \pi \right) S_{Ac} \left(\theta + \imath \frac{h-1}{2h} \pi \right) \right)^{(-1)^{B+c}} = \frac{S_{Ak} \left(\theta + \imath \frac{A+N-k}{h} \pi \right)}{S_{Ak} \left(\theta - \imath \frac{A+N-k}{h} \pi \right)}.$$

To finish, note that the term in (4.8) proportional to K_N receives special treatment, in that it is without the factor of 2 that multiplies all of the others. If $A=2k$, then $b-B$ is odd for this term, and it corresponds to the α -process $A \rightarrow k, k \rightarrow A$, whilst if $A = 2k+1$, $b-B$ is even and the term matches the β -process $A \rightarrow N-k, N-k \rightarrow A$. In both cases the missing 2 is accounted for by a symmetry factor.

The intricate mechanism by which all of the μ -terms are successfully recovered leaves little doubt that equations (4.3) – (4.5) describe exactly the zero-momentum one-particle states at suitably-large values of r . Transitions are inevitable as the ultraviolet regime is approached, and we have already seen examples of the sort of phenomena that can occur. This section ends with one more, showing yet another way in which the equations can change their form in the crossover region.

Consider the first one-particle state in the T_4 theory. As just explained, at large r we expect this to be described by a generalised TBA equation with one pair of active singularities, zeroes of $z_4(\theta)$. These are at $\pm\theta_4^{(0)}$, with $\theta_4^{(0)}$ purely imaginary, tending to $\imath\pi/18$ from above as r grows. Conversely, as r decreases our numerical solutions indicate that $\text{Im}\theta_4^{(0)}$ increases towards $\pi/9$, until at $r_c \approx 2.266315266(7)$ there is a square root singularity in its value as a function of r . This transition is shown in figure 11, and is of the simplest kind seen in previous sections. Decreasing r further, $\theta_4^{(0)}$ starts to run along the line $\text{Im}\theta = \pi/9$, with accompanying zeroes in Y_3 and in Y_4 , both at $\beta_4^{(0)}$, running along the real θ axis. But more importantly, the numerical solution reveals that a so-far inactive singularity also comes

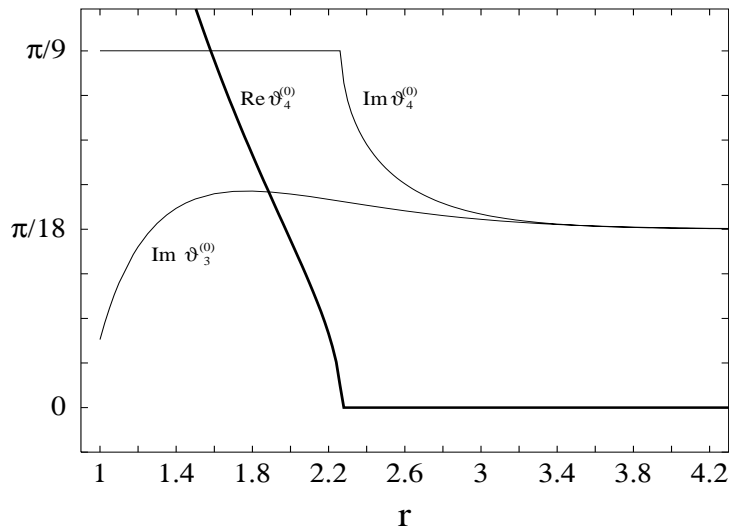


Figure 11: Singularity movement for the first one-particle state in T_4 ($\text{Re } \theta_3^{(0)}$ is equal to 0 for all r in the range plotted, and so this line has been omitted).

into play. This is a zero of $z_3(\theta)$, at $\theta_3^{(0)}$ say, which for large r approaches $i\pi/18$ from above. As r becomes smaller, $\text{Im } \theta_3^{(0)}$ at first grows, reaching a maximum at $r \approx 1.8$, and then decreases, as shown on figure 11. At around $r = 1$, our program became unstable, but extrapolation predicts that at $r \approx 0.9234$ the singularities at $\pm\theta_3^{(0)}$ will cross the real axis and become active. At this stage $\theta_3^{(0)}$ is still on the imaginary θ axis, and a natural scenario for its subsequent movement is that it ultimately reaches $-i\pi/9$, undergoes a transition there and finally runs along the line $\text{Im } \theta = -\pi/9$. The ultraviolet solutions for r real would then have both $\beta_3^{(0)}$ and $\beta_4^{(0)}$ sitting on the real axis, $Y_4(\theta)$ having four zeroes on the real axis, at $\pm\beta_3^{(0)}$ and $\pm\beta_4^{(0)}$, and $Y_3(\theta)$ having two, at $\pm\beta_4^{(0)}$. Via the Y-system, the zeroes of $Y_3(\theta)$ also force $Y_2(\theta)$ to vanish at $\pm\beta_3^{(0)}$. Unfortunately, we have not yet developed the computer code necessary to verify this picture directly. In its absence we can at least make a couple of checks. First, the zeroes just described tell us the signs of the numbers $y_a = Y_a^{\text{kink}}(-\infty)$ for the kink versions of the

solution under discussion, since we already know that $Y^{\text{kink}}(+\infty) = +\infty$:

$$\text{Sign}(y_1, y_2, y_3, y_4) = (+1, -1, -1, +1) .$$

These match the $s=3$, $N=4$ case of the solutions

$$y_a^{(s)} = \frac{\sin(sa\pi/(h+2)) \sin(s(a+2)\pi/(h+2))}{\sin(s\pi/(h+2))^2} \quad (h = 2N+1)$$

to the stationary T_N Y-system, which generalise (3.11). The second check in some senses subsumes the first. Recall from the T_2 discussions that the kink system for the first generalised TBA equation, studied in section 3.3, was alternatively found using the second, excited solution to the ground-state TBA equation on the positive- λ line. For T_4 we found a similar multiplicity of solutions to the ground-state equation. An excited solution to the basic T_4 TBA equation can be found by continuing once anticlockwise around the point $r_0 = \rho_0 e^{11\pi i/36}$, $\rho_0 \approx 1.665(9)$. The limiting singularity pattern of this solution on the positive- λ line $r = \rho e^{11\pi i/36}$ near to $\rho = 0$ turns out to match precisely with the predictions just made on the basis of the assumed transitions in the generalised equation along the real r axis.

Thus not only do singularities become inactive as the ultraviolet is approached, as seen in section 3.5, but also previously inactive singularities can become active. More work will be needed to unravel the full pattern of these transitions, but we have at least exhibited examples of the full range of possibilities.

5 Conclusions

The theories studied in this paper provide a useful set of toy models, on which it has been possible to test and develop the method of analytic continuation of TBA equations advocated in [5].

Although relations with the sine-Gordon model at $\beta^2/8\pi = 2/(2N+3)$ [8], and with the Z_{2N+1} -symmetric conformal theories perturbed by their first thermal operators [3, 11], lend the T_N theories some additional physical interest in their own right, the main objective has been to find general patterns of wider applicability. In the following, we summarise the main results obtained, and indicate some open questions that remain.

- **Shifted conjugation symmetry:** The analyticity of the Y_a 's as functions of the variables a_+ and a_- , near to $a_+ = a_- = 0$, was conjectured

in section 2, and as a consequence the shifted conjugation symmetries (2.9) and (2.11) were deduced. These enabled the TBA equations to be studied in regions where the direct numerical approach failed to converge. In particular, we found in this way that the branch points connecting the various sheets of the Riemann surface are not pinch singularities, but rather arise from the multivalued nature of solutions to individual TBA equations. This contrasts with the ‘free’ behaviour found for the thermally-perturbed Ising model.

- **Singular lines:** Type I and type II singular lines were defined in section 3.2. The type I lines divide the Riemann surface into disjoint regions, within each of which a different generalised TBA equation holds sway. The type II lines are less significant: the TBA equations before and after continuation through these lines can be recast into equivalent forms. As explained in section 3.4, this is reflected in the fact that the crossing of a type I line changes the number of zeroes of the $Y_a(\theta)$ in the strip $|\text{Im } \theta| < \pi/h$, whilst the crossing of a type II line does not. Mapping the pattern of singular lines gives an insight into the relationships between the various generalised TBA systems, and a number of techniques were explored to help in this task. In particular, the result described at the end of section 3.2, based on the ultraviolet splitting of pseudoenergies into kink systems, allows the asymptotic pattern of lines at small r to be controlled on any sheet, just from knowledge of the singularity locations for the relevant set of kink pseudoenergies. So far we have only studied this in detail for the T_N systems, but it is clear that the same picture will hold for any TBA system which splits into separated kink systems in the ultraviolet regime.
- **Exotic solutions to the basic TBA equation:** A basic TBA equation, with no active singularities, has direct access to a series of branch points in the scaling functions. These always turn out to be approximately lined up along the imaginary r axis, as explained for the case of the SLYM in section 3 of ref. [5]. (Figure 4 of that paper shows two of these points for the SLYM, whilst the points A , \tilde{B} and \tilde{D} on figure 1 are three examples from the T_2 theory.) Continuing r anticlockwise around these points, we remain in the domain of validity of the basic TBA, and uncover some previously unsuspected solutions. Furthermore, by returning r to the origin along lines of constant argu-

ment, we found, in sections 3.1 and 3.5, the ‘excited’ kink solutions on the second and third sheets of the T_2 Riemann surface, without ever having to solve a generalised TBA equation. It would be interesting to know whether *all* kink solutions, both in these and other models, can be obtained in this way.

- **Analytic continuation and sum rules:** Continuation in r allows the contours taken in the generalised dilogarithm functions $L_+(\mathcal{C}_a)$ to be determined unambiguously, and in a way which should work completely generally. This has the potential to provide a more ‘physical’ justification for the continuations discussed as purely mathematical properties of dilogarithmic sum rules in [16], and deserves to be studied in greater depth.
- **Desingularisation of the generalised equations:** By explicitly removing the singularities of the pseudoenergies $\varepsilon_a(\theta)$ in the strip $-\pi/h < \text{Im}\theta < \pi/h$ (all related to zeroes of the $Y_a(\theta)$ at the same points) we were able to recast the generalised TBA equations, including the expressions for $c(r)$, into the shape of the basic TBA equations, albeit with redefined functions $\hat{\varepsilon}_a$ and \hat{L}_a . This was very useful for the efficient numerical treatment of the equations, and may be of deeper significance. Note that the identities (3.39) and (3.40) on which the manoeuvre depends hold with trivial modifications for all of the *ADET*-related diagonal scattering theories, and so the technique is immediately applicable to a number of other models.
- **Field theory and the generalised TBA:** In all of the cases that we studied, it proved possible to extract exact asymptotics from the generalised TBA equations which matched the field-theoretic predictions found in refs. [1, 18]. These results relied on a number of intricate identities satisfied by the mass spectra and S-matrices of the T_N -related models. An outstanding problem is to set this into a broader context, and as a first step it would be interesting to know the appropriate generalisations to the other diagonal scattering theories.
- **The crossover region:** The detailed study made in sections 3 and 4 revealed that even for real values of r the generalised TBA equations can change in complicated ways as one moves from the ultraviolet to the infrared, typically undergoing a number of distinct transitions. These transitions can both increase and decrease the number of active

singularities, and as each is passed, a new equation has to be solved. So far we can only appeal to a case-by-case analysis, and more numerical work will probably be needed before a general picture emerges. There is an intriguing similarity between the movements of singularities in the generalised TBA equations and the movements of Bethe ansatz roots near to the scaling limit of lattice models, as studied in ref. [20]; it remains to be seen whether any significance should be attached to this observation.

One item of unfinished business is a study of more general states, even in the T_N models. Based on the experience with the SLYM discussed in ref. [5], it is not hard to guess how to include one-particle states with non-zero spin: the key is to give up the $\theta \rightarrow -\theta$ symmetry of the pseudoenergies, and to replace each pair $\{\theta_a^{(j)}, -\theta_a^{(j)}\}$ of active singularities in the equations previously discussed with a pair $\{\theta_a^{(j)}, \bar{\theta}_a^{(j)}\}$, imposing $\bar{\theta}_a^{(j)} = (\theta_a^{(j)})^*$ whenever r is real. Note that these pairs of singularities belong to either the left or right kink systems from the outset, and so we expect there to be less need for them to undergo transitions as the infrared region is left and the ultraviolet approached. Preliminary studies of the T_2 model show good agreement with results from truncated conformal space, with, so far, no sign of any transitions at all, through the whole range of r . However the full story, both for these states and for states with higher numbers of particles, remains to be uncovered. Numerical problems are rather acute when trying to track more than one or two active singularities, and indeed it is becoming increasingly necessary to develop some alternatives to the rather crude iteration schemes that we have been using to date.

Finally we should mention a hope for the longer term, which is to develop an overall understanding of the Riemann surfaces so far only tentatively explored. There are many structures hidden in these surfaces – in particular we would emphasise their monodromy groups [21] – and it is natural to suppose that these will be related to some of the other pieces of algebraic machinery that enter into the study of integrable quantum field theories.

Acknowledgments — We would like to thank Sergei Lukyanov, John Parker and Francesco Ravanini for useful discussions at various stages, and everyone at the Yukawa Institute, in particular Takeo Inami and Ryu Sasaki, for their hospitality during the early stages of this work. In addition PED would like to thank the Institute Henri Poincaré in Paris and the Institute

for Theoretical Physics in Santa Barbara for hospitality as the project continued. This work was supported in part by a Human Capital and Mobility grant of the European Union, contract number ERBCHRXCT920069, in part by a NATO grant, number CRG950751, in part by a British Council/Royal Society/JSPS joint research project, and in part by the National Science Foundation under grant no. PHY94-07194. PED thanks the EPSRC for an Advanced Fellowship, and RT thanks the Mathematics Department of Durham University for a postdoctoral fellowship.

A Field-theoretic predictions for infrared asymptotics

Finite-size corrections to the energies of one-particle states were studied by Lüscher in ref. [1]. To all orders in perturbation theory, he found that the leading corrections could be expressed in terms of universal quantities appearing in the infinite-volume two-particle S-matrix elements. In this appendix we summarise the results of [1] as applied to the T_N models, drawing also on the convenient and somewhat generalised discussion provided by ref. [18].

If a zero-momentum one-particle state A has a mass equal to M_A on the infinite line, then the mass of the same state on a large but finite circle of circumference R receives corrections from two main sources. Those from the first, called F -terms in [18], give a total contribution

$$\Delta_F M_A = - \sum_b' \frac{M_b}{2\pi} \mathcal{P} \int_{-\infty}^{\infty} d\theta e^{-M_b R \cosh \theta} (S_{Ab}(\theta + i\pi/2) - 1) . \quad (\text{A.1})$$

The prime indicates that terms smaller than the overall error can be dropped (see ref. [18] for more discussion of this point) and the \mathcal{P} signals that the principal part of the integral should be taken. (It is anyway irrelevant for the T_N theories.) These terms can be traced to the interaction of the particle A with a virtual particle b travelling around the space-time cylinder, as illustrated on the left of figure 12.

Contributions of the second type (called μ -terms in [18]) are due to the processes illustrated on the right of figure 12, in which A splits into a pair of virtual particles b and c , which travel around the world before recombining to form A again. The result is proportional to the squares of the on-shell three-point couplings f_{Abc} , and these can be determined from the residues

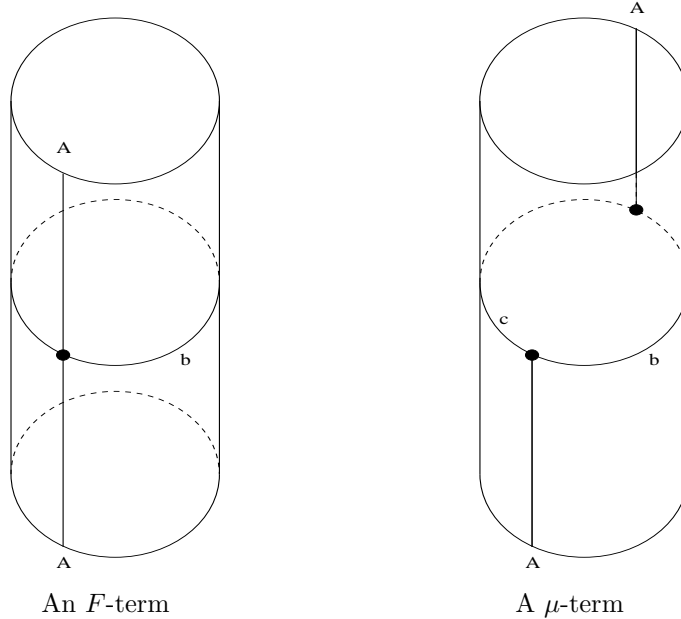


Figure 12: The two classes of diagram responsible for the leading contributions to ΔM_A .

$\mathcal{R}S_{Ab}(\imath U_{Ab}^c)$ of the two-particle S-matrix elements at the appropriate fusing angles $\imath U_{Ab}^c$. The total shift induced by processes of this sort is

$$\Delta_\mu M_A = - \sum'_{b,c} \Theta(M_A^2 - |M_b^2 - M_c^2|) \mu_{Abc} R_{Abc} e^{-\mu_{Abc} R} \quad (\text{A.2})$$

where

$$R_{Abc} = -\imath M_{Abc} \mathcal{R}S_{Ab}(\imath U_{Ab}^c), \quad (\text{A.3})$$

and

$$\mu_{Abc} = M_b \sin U_{Ab}^c = M_c \sin U_{Ac}^b = \frac{M_b M_c}{M_A} \sin U_{bc}^A. \quad (\text{A.4})$$

In these definitions, M_{Abc} is one if $f_{Abc} \neq 0$ and zero otherwise, and the step function

$$\Theta(x) = \begin{cases} 0 & \text{if } x < 0 \\ \frac{1}{2} & \text{if } x = 0 \\ 1 & \text{if } x > 0 \end{cases}$$

serves to disqualify those virtual processes $A \rightarrow bc \rightarrow A$ which cannot be drawn as on-shell diagrams on the cylinder.

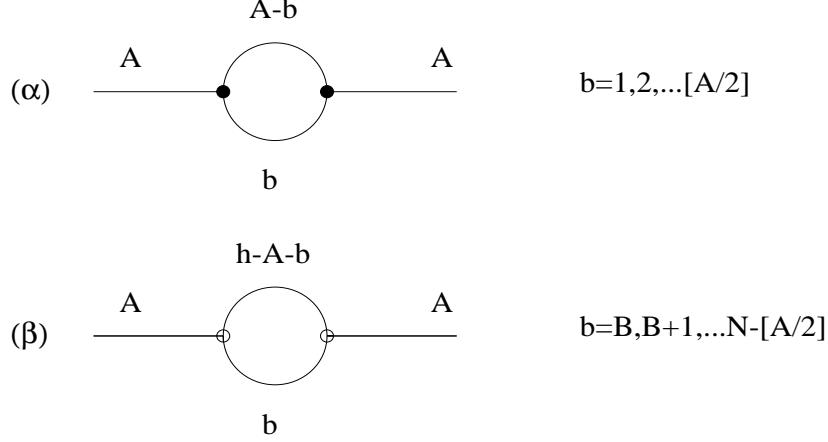


Figure 13: A set of μ -terms in the T_N theory.

Specialising to the non-unitary T_N theories, the non-vanishing couplings are as follows:

$$\begin{aligned} f_{Abc} &\in \mathbb{R}^* && \text{if } c = A+b \leq N \text{ or } c = |A-b| \neq 0; \\ f_{Abc} &\in i\mathbb{R}^* && \text{if } c = h - (A+b) \leq N; \\ f_{Abc} &= 0 && \text{otherwise,} \end{aligned}$$

and the fusing angles are

$$\begin{aligned} U_{Ab}^{|A-b|} &= \left(1 - \frac{|A-b|}{h}\right) \pi; \\ U_{Ab}^{n(A,b)} &= \left(\frac{A+b}{h}\right) \pi, \end{aligned}$$

with $n(A,b) = \min(A+b, h-A-b)$. Due to the step function in (A.2), only the contributions corresponding to the diagrams represented in figure 13 are non-vanishing, and these give

$$\begin{aligned} \mu_{A,b,A-b} &= m_b \sin\left(\frac{|A-b|}{h}\pi\right), \\ R_{A,b,A-b} &= -i\mathcal{R}S_{Ab}\left(i\left(1 - \frac{|A-b|}{h}\right)\pi\right), \quad b = 1, 2, \dots [A/2] \end{aligned} \quad (\text{A.5})$$

for α -processes, and

$$\begin{aligned} \mu_{A,b,h-A-b} &= m_b \sin\left(\frac{A+b}{h}\pi\right), \\ R_{A,b,h-A-b} &= -i\mathcal{R}S_{Ab}\left(i\frac{A+b}{h}\pi\right), \quad b = B, B+1, \dots N-[A/2] \end{aligned} \quad (\text{A.6})$$

for β -processes. Note that the two types of process contribute oppositely to $\Delta_\mu M_A$, since the couplings involved in the α -processes are real, while those in the β -processes are purely imaginary. The total number of distinct contributions is equal to A , which is reflected in the fact that there are A independent active singularities in the relevant generalised TBA equation.

B Numerical results

In this appendix, numerical solutions to the excited-state TBA equations discussed in section 3 are compared with TCSA data. For the first one-particle state, table 1 was compiled using equations (3.44) – (3.47), and table 2 using equations (3.22), (3.23) and (3.26). For the second one-particle state, table 3 used using (3.71), (3.72), and tables 4 and 5, (3.73) – (3.75). Table 5 was also checked using (3.65) – (3.67). Accuracies for the TBA results were estimated by varying parameters such as the discretisation of the θ axis until the results stabilised at the quoted values, whilst accuracies for the TCSA were estimated by varying the truncation level. The first TBA entry in table 4 was obtained by extrapolation from larger values of r , since our iterative routine failed to converge there.

r	TBA	TCSA	$\beta_2^{(0)}$
0.25	0.23816052575(2)	0.23816052577(4)	2.44086172191(0)
0.50	0.23856619676(8)	0.2385661967(3)	1.74875349244(1)
0.75	0.23957858011(5)	0.23957857(9)	1.34585654321(1)
1.00	0.24140149459(4)	0.24140149(2)	1.06270397320(0)
1.25	0.24415555107(8)	0.2441555(4)	0.84614229277(0)
1.50	0.24785826484(5)	0.2478582(4)	0.67206426675(5)
1.75	0.25241760010(3)	0.252417(5)	0.52676984074(1)
2.00	0.25764227087(8)	0.257642(1)	0.40064138633(5)
2.25	0.26326448567(0)	0.263264(2)	0.28454565858(0)
2.50	0.26896728571(2)	0.268967(1)	0.16239328864(9)

Table 1: First one-particle level, $r < r_c$.

r	TBA	TCSA	$i\beta_2^{(0)}$
2.75	0.27440978264(3)	0.274409(3)	0.10660570253(6)
3.00	0.27924699310(4)	0.279246(3)	0.19389451747(5)
3.25	0.28314394898(6)	0.283143(1)	0.23644517085(6)
3.50	0.28578526162(5)	0.28578(4)	0.26216147499(3)
3.75	0.28688156615(0)	0.28688(0)	0.27879066486(6)
4.00	0.28617389043(3)	0.28617(2)	0.28989626682(7)
4.25	0.28343648042(0)	0.28343(4)	0.29744353109(2)
4.50	0.27847823059(8)	0.27847(6)	0.30262252477(1)
4.75	0.27114269310(0)	0.27114(0)	0.30619467150(4)
5.00	0.26130666042(9)	0.26130(4)	0.30866417603(4)
5.25	0.24887745081(7)	0.24887(5)	0.31037226542(4)
5.50	0.23378918672(7)	0.23378(7)	0.31155300241(8)
5.75	0.21599846946(4)	0.21599(6)	0.31236819753(5)
6.00	0.19547988038(6)	0.19547(9)	0.31293014812(8)
7.00	0.08602148615(6)	0.08602(7)	0.31388982426(3)
8.00	-0.06688310507(3)	-0.0668(6)	0.31410090210(8)
10.0	-0.50050238863(1)	-0.500(4)	0.31415656313(2)
15.0	-2.31926770945(7)	-2.31(8)	0.31415926412(7)
20.0	-5.18417167922(3)	-5.18(2)	0.31415926535(8)
30.0	-14.0517103842(1)	-14.0(4)	0.31415926535(8)

Table 2: First one-particle level, $r > r_c$.

r	TBA	TCSA	$\beta_1^{(0)}$
0.25	0.8095238098(2)	0.80952380986(1)	3.2949747170(7)
0.50	0.8095238271(8)	0.8095238272(2)	2.6018275552(3)
0.75	0.8095239881(9)	0.8095239882(1)	2.1963626206(8)
1.00	0.8095247257(6)	0.8095247258(0)	1.9086813430(7)
1.25	0.8095270410(0)	0.8095270410(7)	1.6855402842(2)
1.50	0.8095327731(5)	0.809532773(2)	1.5032248871(9)
1.75	0.8095448001(5)	0.809544800(3)	1.3490870895(8)
2.00	0.8095670652(3)	0.809567065(4)	1.2155794073(0)
2.25	0.8096043028(5)	0.80960430(4)	1.0978356190(0)
2.50	0.8096613348(7)	0.80966133(5)	0.9925341024(8)
2.75	0.8097417885(7)	0.80974178(9)	0.8973043325(8)
3.00	0.8098461844(7)	0.80984618(3)	0.8103904953(7)
3.25	0.8099693378(1)	0.80996933(8)	0.7304470394(3)
3.50	0.8100972214(6)	0.81009722(2)	0.6564058765(0)
3.75	0.8102034874(6)	0.8102034(9)	0.5873835438(9)
4.00	0.810246050(1)	0.8102460(6)	0.522609957(4)
4.25	0.810164185(2)	0.810164(2)	0.461365983(5)
4.50	0.809876615(7)	0.809876(7)	0.402917258(4)

Table 3: Second one-particle level, $r < r_{c1}$.

r	TBA	TCSA	${}_i\beta_1^{(0)}$	$-{}_i\theta_2^{(0)}$
4.75	0.8092809(5)	0.80928(1)	0.346424(5)	0.015804(6)
5.00	0.80825467(3)	0.80825(5)	0.29078538(8)	0.10280614(0)
5.25	0.80665753(1)	0.80665(8)	0.23427070(8)	0.14891716(3)
5.50	0.80433518(4)	0.80433(6)	0.17338533(0)	0.18056955(6)
5.75	0.80112353(4)	0.80112(4)	0.09649407(3)	0.20409098(1)

Table 4: Second one-particle level, $r_{c_1} < r < r_{c_2}$.

r	TBA	TCSA	${}_i\beta_1^{(0)}$	$-{}_i\theta_2^{(0)}$
6.00	0.7968556702(0)	0.79685(7)	0.0896301999(2)	0.2223149258(0)
6.25	0.7913547600(8)	0.79135(9)	0.1501055922(9)	0.2368163134(7)
6.50	0.7844612122(0)	0.78446(8)	0.1861508713(2)	0.2485780614(9)
6.75	0.7760128576(7)	0.7760(2)	0.2116358291(4)	0.2582559981(1)
7.00	0.7658591165(7)	0.7658(7)	0.2308123309(7)	0.2663096804(3)
7.25	0.7538605345(2)	0.7538(8)	0.2457260952(8)	0.2730722975(5)
7.50	0.7398899544(4)	0.739(9)	0.2575655998(7)	0.2787920410(3)
7.75	0.7238331001(3)	0.723(8)	0.2670979493(9)	0.2836579633(7)
8.00	0.7055886730(5)	0.705(6)	0.2748522116(1)	0.2878168593(0)
8.50	0.6621947642(6)	0.662(2)	0.2864555943(6)	0.2944542899(1)
9.00	0.6091397136(7)	0.609(2)	0.2944284302(9)	0.2993877628(7)
10.0	0.4725672915(3)	0.472(7)	0.3039279521(5)	0.3058454231(1)
15.0	-0.8450264306(8)	-0.84(3)	0.3136882646(6)	0.3137048805(9)
20.0	-3.2169979044(2)	-3.21(5)	0.3141349870(6)	0.3141351300(9)
30.0	-11.100815854(4)	-1(4)	0.3141591977(4)	0.3141591977(4)

Table 5: Second one-particle level, $r > r_{c_2}$.

References

- [1] M.Lüscher, ‘Volume dependence of the energy spectrum in massive quantum field theories. 1. Stable particle states’, *Comm. Math. Phys.* **104** (1986) 177.
- [2] M.Lüscher, ‘Volume dependence of the energy spectrum in massive quantum field theories. 2. Scattering states’, *Comm. Math. Phys.* **105** (1986) 153;
M.Lüscher and U.Wolff, ‘How to calculate the elastic scattering matrix in two-dimensional quantum field theories by numerical simulation’, *Nucl. Phys.* **B339** (1990) 222.
- [3] Al.B.Zamolodchikov, ‘Thermodynamic Bethe Ansatz in Relativistic Models. Scaling 3-state Potts and Lee-Yang Models’, *Nucl. Phys.* **B342** (1990) 695.
- [4] V.V.Bazhanov, S.L.Lukyanov and A.B.Zamolodchikov, ‘Integrable quantum field theories in finite volume: excited state energies’, *Nucl. Phys.* **B489** (1997) 487.
- [5] P.Dorey and R.Tateo, ‘Excited states by analytic continuation of TBA equations’, *Nucl. Phys.* **B482** (1996) 639.
- [6] D.Fioravanti, A.Mariottini, E.Quattrini and F.Ravanini, ‘Excited state Destri–de Vega equation for sine-Gordon and restricted sine-Gordon models’, *Phys. Lett.* **B390** (1997) 243;
C.Destri and H.J.de Vega, ‘Nonlinear integral equation and excited states scaling functions in the sine-Gordon model’, preprint PAR-LPTHE-96-46, IFUM-546-FT, hep-th/9701107 (Jan 1997).
- [7] J.L.Cardy and G.Mussardo, ‘ S matrix of the Yang-Lee edge singularity in two-dimensions’, *Phys. Lett.* **B225** (1989) 275;
P.G.O.Freund, T.R.Klassen and E.Melzer, ‘ S -matrices for perturbations of certain conformal field theories’, *Phys. Lett.* **B229** (1989) 243.
- [8] F.Smirnov, ‘Reductions of the sine-Gordon model as a perturbation of minimal models of conformal field theory’, *Nucl. Phys.* **B337** (1990) 156.
- [9] Al.B.Zamolodchikov, ‘Mass scale in sine-Gordon model and its reductions’, *Int. J. Mod. Phys.* **A10** (1995) 1125.

- [10] V.P.Yurov and Al.B.Zamolodchikov, ‘Truncated conformal space approach to the scaling Lee-Yang model’, *Int. J. Mod. Phys.* **A5** (1990) 3221.
- [11] T.R.Klassen and E.Melzer, ‘Purely elastic scattering theories and their ultraviolet limits’, *Nucl. Phys.* **B338** (1990) 485;
 ———, ‘The thermodynamics of purely elastic scattering theories and conformal perturbation theory’, *Nucl. Phys.* **B350** (1991) 635.
- [12] Al.B.Zamolodchikov, ‘On the thermodynamic Bethe ansatz equations for the reflectionless ADE scattering theories’, *Phys. Lett.* **B253** (1991) 391.
- [13] F.Ravanini, R.Tateo and A.Valleriani, ‘Dynkin TBAs’, *Int. J. Mod. Phys.* **A8** (1993) 1707.
- [14] M.Lässig and G.Mussardo, ‘Hilbert space and structure constants of descendant fields in two-dimensional conformal theories’, *Computer Phys. Comm.* **66** (1991) 71.
- [15] A.Klümper, T.Weher and J.Zittartz, ‘Conformal spectrum of the six-vertex model’, *J. Phys.* **A26** (1993) 2815.
- [16] A.Kuniba and T.Nakanishi, ‘Spectra in conformal field theories from the Rogers dilogarithm’, *Mod. Phys. Lett.* **A7** (1992) 3487.
- [17] A.Klümper and P.A.Pearce, ‘Analytic calculation of scaling dimensions: tricritical hard squares and critical hard hexagons’, *J. Stat. Phys.* **64** (1991) 13.
- [18] T.R.Klassen and E.Melzer, ‘On the relation between scattering amplitudes and finite-size mass corrections in QFT’, *Nucl. Phys.* **B362** (1991) 329.
- [19] R.J.Eden, P.V.Landshoff, D.I.Olive and J.C.Polkinghorne, *The analytic S-matrix*, Cambridge at the University Press, 1966.
- [20] U.Grimm and B.Nienhuis, ‘Scaling limit of the Ising model in a field’, *Phys. Rev.* **E55** (1997) 5011.
- [21] See, for example, C.L.Siegel, *Topics in complex function theory vol. 1*, Wiley-Interscience 1969, page 101.